Reviews of Geophysics

REVIEW ARTICLE
10.1029/2020RG000722

Key Points:

- Laminated stalagmites are characterized by centennial-scale stability in accumulation rate
- Strong multi-year climate signals may retain an imprint in annual growth rate after smoothing of this signal by mixing with stored water
- Long-term constant growth rate of laminated stalagmites benefits accurate chronology building

Supporting Information:

Supporting Information may be found in the online version of this article.

Correspondence to:

A. Baker,
a.baker@unsw.edu.au

Citation:

Baker, A., Mariethoz, G., Comas-Bru, L., Hartmann, A., Frisia, S., Borsato, A., et al. (2021). The properties of annually laminated stalagmites-A global synthesis. *Reviews of Geophysics*, *59*, e2020RG000722. https://doi.org/10.1029/2020RG000722

Received 29 OCT 2020
Accepted 7 FEB 2021

The Properties of Annually Laminated Stalagmites-A Global Synthesis

Andy Baker[1,6], Gregoire Mariethoz[2], Laia Comas-Bru[3], Andreas Hartmann[4,1], Silvia Frisia[5], Andrea Borsato[5], Pauline C. Treble[6,1], and Asfawossen Asrat[7]

[1]School of Biological, Earth and Environmental Sciences, UNSW Sydney, Sydney, NSW, Australia, [2]Institute of Earth Surface Dynamics (IDYST), University of Lausanne, Lausanne, Switzerland, [3]School of Archaeology Geography and Environmental Science, University of Reading, Reading, UK, [4]Chair of Hydrological Modeling and Water Resources, Albert-Ludwigs-University of Freiburg, Freiburg, Germany, [5]School of Environmental and Life Sciences, The University of Newcastle, Callaghan, NSW, Australia, [6]ANSTO, Lucas Heights, NSW, Australia, [7]School of Earth Sciences, Addis Ababa University, Addis Ababa, Ethiopia

Abstract Annually laminated speleothems have the potential to provide information on high-frequency climate variability and, simultaneously, provide good chronological constraints. However, there are distinct types of speleothem annual laminae, from physical to chemical, and a common mechanism that links their formation has yet to be found. Here, we analyzed annually laminated stalagmites from 23 caves and 6 continents with the aim to find if there are common mechanisms underlying their development. Annually laminated stalagmites are least common in arid and semiarid climates, and most common in regions with a seasonality of precipitation. At a global scale, we observe faster growth rates with increasing mean annual temperature and decreasing latitude. Changepoints in average growth rates are infrequent and age-depth relationships demonstrate that growth rates can be approximated to be constant. In general, annually laminated stalagmites are characterized by centennial-scale stability in calcite precipitation due to a sufficiently large and well-mixed water source, a time series spectrum showing first-order autoregression due to mixing of stored water and annual recharged water, and an inter-annual flickering of growth acceleration, bringing growth rates back to the long-term mean. Climate forcing of growth rate variations is observed where a multi-year climate signal is strong enough to be the dominant control on calcite growth rate variability, such that it retains a climate imprint after smoothing of this signal by mixing of stored water. In contrast, long-term constant growth rate of laminated stalagmites adds further robustness to their unparalleled capacity to improve accuracy of chronology building.

Plain Language Summary Growth layers, or laminae, are found in many biological and geological records. Stalagmites, mineral precipitates found in caves, can contain annual laminae. Stalagmites grow upwards from water which drips onto them from overlying fractures and voids. For annually laminated stalagmites, it is not known where and for how long they form, and why. Here, we review and statistically analyze a global data set of laminated stalagmites. They are less common in water-limited climates and are only found in regions with seasonal precipitation. The annual average laminated stalagmite vertical growth is 0.093 mm, increasing with warmer temperatures. Stalagmite accumulation rate is relatively unchanging over time. This is because their drip water source has enough volume and a stable chemical composition to be a buffer to rapid changes. Year-to-year, we see a "flickering," where accumulation rate returns toward the long-term average, also due to this buffering effect. For an environmental signal to be preserved in stalagmite laminae thickness requires a large perturbation, such as wet or dry years associated with the El Niño-Southern Oscillation, that can override the buffering of the overlying water source. The long-term constant growth rate of laminated stalagmites provides an unparalleled capacity for precise chronology building.

1. Introduction

Annually resolved proxy records of past climate variability enable assessment of high-frequency and low-frequency periodicities that allow recognition of how external climate forcing (such as solar variability or volcanic forcing) influences climate drivers (such as the El Niño-Southern Oscillation [ENSO], Indian

Ocean Dipole [IOD] or North Atlantic Oscillation [NAO]). (See Glossary for the definition of all terminology). Studies of annually laminated archives such as ice cores, marine and lake sediments, and trees, are relatively common while they have been relatively unexploited in speleothems. Here, we briefly review the annually laminated archives from ice cores, marine and lake sediments, and trees, to place the annually laminated speleothem record into context.

In the polar regions, ice cores have yielded 800,000 years of Antarctic climatic variability; atmospheric and methane CO_2 concentrations revealing the range of natural variability and demonstrating connections between Antarctica and distant locations across the entire Earth (Barker et al., 2011; E. J. Brook & Buizert, 2018). However, for Greenland the annual lamina record is 60,000 years (Lemieux-Dudon et al., 2010) and the Epica Dome C age model is generated by combining several age markers and glaciological models (Parrenin et al., 2007). The geochronological control among Antarctica and Greenland ice cores is complicated by the fact that annual laminae are not preserved in deep ice cores, due to their thinning with glacier flow and glaciological models must be used, which leaves room for improvement of the age synchronization between the network of ice cores (E. J. Brook & Buizert, 2018). Critically, stalagmite precise age dating of climate events allowed tuning of timing and duration of the same stadials in Greenland and Antarctica ice core records beyond 60,000 years ago (Drysdale et al., 2007, 2009).

Outside the polar ice caps, annually laminated sediments allow insight on past climate from the present-day to millions of years ago. These include lacustrine and marine varved sediments, and speleothems. There are also annually laminated biological archives, which can be preserved in the geologic record, such as corals and tree rings. All provide an annually resolved geochronology and information on different processes that have influenced Earth's climate. Marine varved sediments are preserved in anoxic basins. The best example is from the Cariaco Basin, the laminated cores which cover much of the last 90,000 years (Peterson et al., 2000). Dating is critical for the older parts of the laminated sediments and is commonly relying on radiocarbon and varve counting via multiple techniques, given that varves are not always annual. Varved marine sediments are most apt to capture regional fluvial discharge, local upwelling intensity, and sea surface temperature (SST; Black et al., 2007; Peterson & Haug, 2006; Staubwasser et al., 2003).

Remaining in the marine environment, the biological record related to annual coral skeleton growth provides unparalleled insight on SST in the tropical ocean, thus expanding our understanding of climate changes associated with ENSO and/or IOD (Tierney et al., 2015). However, the lifespan of corals means that coral skeleton growth laminae do not grow uninterruptedly for thousands or hundreds of thousands of years. Thus, precise ages for fossil corals must be obtained by anchoring these lamina chronologies using U-series dating, where errors associated with age determinations have been demonstrated to be less than 1% for well-preserved, last interglacial coral samples (Bard et al., 1990). One of the biggest issues with dating corals is the fact that they are commonly subject to diagenesis, where dissolution and re-precipitation results in age uncertainties for old coral reefs.

In the continental environment, varved lake sediments have allowed insight on the dynamics of abrupt climate changes at least for the last 70,000 years (Brauer et al., 2008; Sirocko et al., 2013; Zolitschka et al., 2015). They form because of a seasonality of depositional processes from the water column and/or of transport from the catchment area. The preservation of laminae depends on sustained absence of sediment mixing due to waves and/or bioturbation and/or methane gas bubbles that may disrupt varves (Zolitschka et al., 2015). The preservation of varved sediments, thus, requires lakes with an anoxic bottom, in a stable tectonic setting and in regions where there is strong seasonal contrast, particularly in temperature. Therefore, long, continuous, accurate varve chronologies extending over 100 years are mostly found in the mid to high latitudes of the Northern Hemisphere but are rare in the equatorial regions and in the Southern Hemisphere (cf. Wolff et al., 2011; Zolitschka et al., 2015).

The biologic equivalent of corals in continental settings are tree rings. Most commonly, tree rings are routinely used to reconstruct high-resolution last millennium climate variability. Floating tree ring chronologies allow us to gain rare insight into earlier periods (Muscheler et al., 2008). For example a South American conifer floating 1,229-year chronology has allowed paleoclimate data to be obtained back to ~50,000 ^{14}C-years before present (Roig et al., 2001). However, tree ring chronologies and paleoclimate information, like that obtained from varved sediments in lakes and corals, are best obtained from regions where there

is a strong seasonal contrast (mostly temperature and hydrology). Furthermore, most tree-ring studies are unlikely to extend the chronology well beyond the Holocene.

A promising continental archive of long, uninterrupted, climate-related proxy data that encompasses all latitudes outside the polar regions and may provide annual time series of rainfall and/or temperature in habitable lands are laminated speleothems (secondary mineral deposits in caves) that can be analyzed at sub-annual resolution. Although only a subset of speleothems has been observed to contain physical (visible) laminae formed from changes in fabric/porosity, increasing use of high-resolution elemental mapping is revealing the more widespread occurrence of chemical laminae (Woodhead et al., 2010). One of the most important properties of caves is that they are a conservative system, capable of preserving its mineral deposits unaltered for hundreds of thousands of years and longer (Vaks et al., 2020; Woodhead et al., 2019). This means that diagenetic alteration, specifically calcite to calcite recrystallization, is not common. And aragonite to calcite transformation, which affects corals, is distinguishable by petrographic investigation and is relatively uncommon (Bajo et al., 2016 and references herein). Furthermore, perturbations of the stratigraphic order are not to be expected as in varved sediments because speleothem layers are already mineralized, the record is not as fragmentary as for tree-rings (and corals), and can be temporally constrained by accurate uranium-series and/or radiocarbon radiometric dating (Holmgren et al., 1994; Hua et al., 2012) and/or annual trace element cycles (Nagra et al., 2017).

Speleothem annual laminae were first recognized through UV fluorescence and/or optical microscopy observation of particulate, both originated from different degrees of decomposition of soil-derived organic material (Baker et al., 1993; Frisia et al., 2003; Shopov et al., 1994), and from seasonal variations in calcite fabric or mineralogy (Broecker et al., 1960; Genty, 1993). More recently, advances in high-resolution elemental mapping have enabled the identification of annual variability in trace elements, mostly commonly Sr (Borsato et al., 2019), but also Mg, Na, H, Ba, Y, P, Br, etc. (Borsato et al., 2007; Fairchild et al., 2001; Smith et al., 2009). For exceptionally fast-growing stalagmites, micromilling or in situ techniques can provide seasonally resolved data for carbon and oxygen isotopes that reveal annual variability (Mattey, 2010; Myers et al., 2015; Orland et al., 2014; Ridley et al., 2015; Treble et al., 2005). The majority of published records to date are of short duration (<100 years, the one exception is Ridley et al. [2015]), reflecting the time-consuming sampling and analysis required to construct long isotope records at this resolution.

The main criterion used to confirm the annual periodicity of laminae are comparison with radiometric dating methods such as uranium-thorium (Dominguez-Villar et al., 2012) or radiocarbon age determinations (if a constant contribution of host rock carbon is likely; Broecker et al., 1960), and for recently deposited samples, identification of the 1960s atmospheric nuclear testing as peaks of radiocarbon (Mattey et al., 2008) or 137-Cesium (Frappier et al., 2007) where it is possible. In addition, where cave monitoring is possible, the annual growth rate (or vertical extension rate, see Glossary) represented by the laminae of recently deposited stalagmites can be compared to that theoretically predicted for the observed drip hydrology, cave climate, and drip water chemistry (Dreybrodt, 1999), and in situ calcite growth experiments can also be used to confirm the annual nature of lamina deposition (Frisia et al., 2000). These approaches can be complimented by observations of lamina properties in thin-section, which can be used to identify the possible presence of dissolution features and micro-hiatuses that might represent the location of missing laminae.

Speleothems, therefore, have been observed to primarily include four different annual lamina types. Physical (visible) laminae are formed from (i) calcite fabric/porosity and (ii) from particulate, or colloidal, organic matter concentration annual variability. Chemical laminae consist of both organic and inorganic cycles as (iii) changes in fluorescence under ultra-violet excitation, occurring due to the intrinsic fluorescence of some organic matter fractions and (iv) as annual variations in trace element or oxygen and carbon isotope content. Our observations are that fabric laminae usually also have chemical cycles and can exhibit fluorescence; that particulate - colloidal organic matter laminae are also fluorescent and exhibit chemical cycles; and that fluorescent laminae usually also exhibit chemical cycles. Examples are presented in Figure 1.

Another way to group laminae types is based on the process of lamina formation itself, whether hydrologically controlled or cave-climate controlled. Annual laminae preserved in strontium (Sr) and other trace elements, particles, and fluorescent organic matter concentration variations are directly related to hydrological

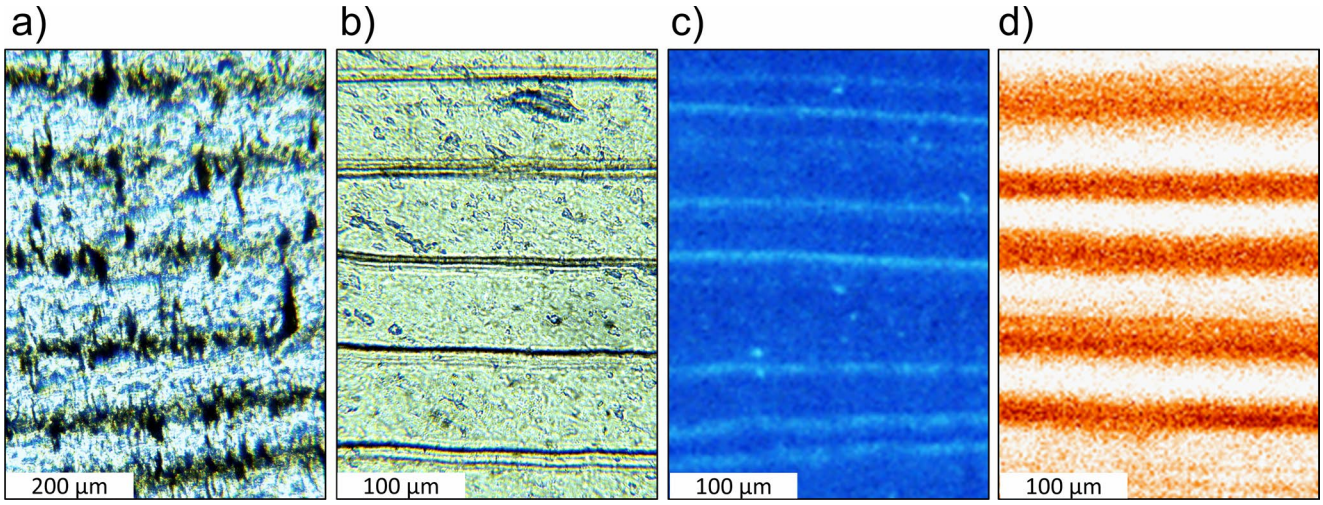

Figure 1. Laminae types. (a) Thin section of calcite fabric/porosity laminae. (b) Thin section of particulate—colloidal organic matter (optically visible); each hydrological year is marked by a 1–4 µm-thick brown lamina often accompanied by a variable number of thinner sub-annual laminae. (c) Thin section of fluorescent organic matter laminae under UV excitation. (d) Chemical laminae (strontium) as mapped by synchrotron radiation—µXRF. Lamina types are not exclusive: fabric laminae can also have chemical cycles and can exhibit fluorescence; particulate—colloidal organic matter laminae are also fluorescent and exhibit chemical cycles, while fluorescent laminae usually exhibit chemical cycles.

controls. Specifically, organic matter, particulate, and colloidal laminae reflect a seasonal transport of soil-derived material, typically in the wet season. Strontium concentrations, which are commonly derived from host rock dissolution, forms laminae when there is seasonal variation in extent of rock-water interaction or precipitation of Sr-depleted calcite along the hydrological flow path to the speleothem, also known as prior calcite precipitation (PCP). In contrast, the preservation of physical annual laminae in speleothems, producing fine texture or fabric alternation, are thought to be controlled by both seasonal ventilation (and associated changes in cave air pCO_2) and the competition between subsequent water supersaturation state with respect to calcium carbonate and inflow from the surface of compounds and/or ions that influence crystallization (Frisia et al., 2000). This competition affects crystal growth by blocking growth sites when supersaturation is low and impurities are high (Frisia et al., 2000). Seasonality in cave climate would be expected to be strongest in mid- to high-latitude and high-altitude regions characterized by strong seasonal temperature contrast (James et al., 2015). The amount of annual vertical extension preserved in laminae to give a speleothem growth rate can, therefore, relate to the hydrological year or the cave climate year. The extent of any difference in annual growth rate characteristics between different laminae types (fabric vs. trace element) has yet to be investigated. Do stalagmites with laminae from carbonate fabric variations have different annual growth rate properties and climate sensitivity compared to other lamina types with a direct hydrological control?

Speleothem annual growth rate is determined by multiple environmental processes. The primary control on calcite growth rate is the supersaturation state of the drip water with respect to this $CaCO_3$ phase (Buhmann & Dreybrodt, 1985), although a high concentration of impurities in a supersaturated parent water, for example Mg, slows down calcite growth (Davis et al., 2000). Supersaturation with respect to calcite is influenced by the extent of dissolution of the carbonate bedrock, typically limestone and/or dolomite. This extent of dissolution is usually determined by the production of carbon dioxide from soil and ground air microbial communities and tree root respiration that combine with water to form the carbonic acid. It is also determined by the extent of PCP and the concentration of carbon dioxide in the cave air (Fairchild & Baker, 2012). The carbon dioxide concentration of the cave atmosphere can also affect growth rates, with a slower speleothem growth rate at higher cave atmospheric CO_2 concentrations. Water supply (drip rate) provides a direct hydrological control on growth rate of stalagmites, with limited growth possible at both very slow and very fast drip rates. At very slow drip rates, drip intervals are longer than the time taken for calcite formation and at very high flow rates, degassing is incomplete (Hartmann & Baker, 2017). Temperature has a control on the reaction rate of calcite formation, although this is dominated by the temperature control on soil and vegetation CO_2 productivity (Borsato et al., 2015).

Speleothem annual growth rate time series have found two applications in paleoclimate research. The first is providing annual climate reconstructions, where variations in annual growth rate correlate with a climate forcing. The second is the use of the annual laminae to produce accurate geochronological controls between radiometrically dated layers.

Applications where climate reconstructions have been achieved from speleothem annual growth rate include reconstructions of the NAO (Baker et al., 2015; Trouet et al., 2009), ENSO (Rasbury & Aharon, 2006), Chinese monsoon climate (Tan et al., 2003), and mean annual temperature (MAT) reconstruction and solar forcing (Frisia et al., 2003). The NAO reconstructions are from Uamh an Tartair (Cave of the Roaring) in Scotland, which has a peat bog above the cave. The relative water saturation of the soil drives growth rate (wetter conditions fully saturate the peat, which decrease soil CO_2 productivity and associated limestone dissolution, leading to a slow speleothem growth rate). This climatic control on limestone dissolution dominates over direct hydrological effects on changes in drip rate. The record from Shihua Cave, near Beijing within the northern sector of the Chinese monsoon region, suggests that stalagmite growth rate correlates with climate, but in the opposite direction (warm and wet leads to more CO_2 production, faster dripping, and faster stalagmite growth). Similarly, Rasbury and Aharon (2006) used annual-lamina chronologies in modern Niuean stalagmites to identify a dominant and positive precipitation control on growth rate, and thus reconstruct a role for ENSO as a driver of rainfall variability over multi-year timescales.

Annual laminae time-series can be used to reconstruct age-depth profiles, upon which the chronologies of other proxy records can be accurately placed. A standard approach is to use U-Th analyses to temporally constrain floating annual-lamina chronologies. This has utility when investigating high-resolution (multi-year to centennial) climate variability, for which accurate chronological control is needed. For example, Frappier et al. (2007) used annual fabric lamina chronology to associate oxygen isotopic ratio excursions from a modern Belize stalagmite with tropical cyclones. Belli et al. (2013) used particulate organic matter laminae to bracket the duration of cold-dry conditions associated with the Younger Dryas event in a stalagmite from Northern Italy. Badertscher et al. (2014) used chemical laminae to date the Santorini Minoan eruption in a Turkish stalagmite, thus supporting an independent composite dendrochronology reconstruction. Liu et al. (2015) use stalagmites with both fluorescent and fabric laminae from the monsoon climate region of China to constrain oxygen isotope time series, with the annual temporal resolution permitting investigation of centennial-scale changes in monsoon intensity. Flohr et al. (2017) used annual fabric laminae to constrain a high-resolution isotope record for the last 2,400 years in northern Iraq, identifying past multi-decadal and long-term droughts, and the role of aridification in the rise and fall of regional civilizations.

Over recent decades, individual and community initiatives to archive paleoclimate data has led to the online storage of numerous annual growth rate time series, which include the World Data Service for Paleoclimatology, part of the NOAA National Centers for Environmental Information (NCEI) repository. More recently, annual growth rate time series have been archived as part of the Speleothem Isotope Synthesis and Analysis (SISAL) database of speleothem carbon and oxygen isotope ratios ($\delta^{13}C$ and $\delta^{18}O$), in the instances where annual laminae provide the age-depth geochronology. Combined with some additional unarchived or unpublished growth rate time series, there is now a global data set of stalagmite annual growth rate time series that can be investigated to (1) increase our understanding of the relative importance of the various potential climate and hydrological controls on laminated stalagmite type, growth rates and duration (2) use long-term stalagmite growth rates in geochronological applications.

2. Methods

2.1. Data Compilation

We compiled a database of annually laminated speleothem time series using a combination of database searches and previously unpublished data. Annual laminations were identified as either physical laminations (annual changes in calcite fabric or micro-particulate organic matter inclusions) or chemical laminations (annual changes in trace element composition or fluorescent organic matter). Fabric laminae can include phase laminae (e.g., seasonal alternations in calcite and aragonite, G. A. Brook et al., 1999) and annual changes in aragonite fabric (e.g., Duan et al., 2012), but no archived time series were identified for these

lamina types. The two databases investigated were the SISAL v2 database (Comas-Bru, Atsawawaranunt, et al., 2020; Comas-Bru, Rehfeld, et al., 2020) and the NOAA World Data Centre—Paleoclimate.

Metadata for each speleothem and associated cave was compiled for the type of lamina and their climatic interpretation (if any); geolocation data (latitude, longitude, altitude of the cave, cover thickness and host-rock age and lithology); modern hydroclimate data (MAT, total annual precipitation, potential evapotranspiration [PET], and Aridity Index [AI; from Worldclim v1, Zomer et al., 2007, 2008], seasonality of precipitation [using the Seasonality Index of Walsh and Lawler, 1981; see Glossary]). Historical temperature and precipitation data for the period 1901–2019 CE was extracted from the CRU TS4.04 gridded data set (Harris et al., 2020). Recharge amount and karst storage was modeled using a global recharge model specialized for karst regions (Hartmann et al., 2020), and seasonality of recharge determined (applying the Walsh & Lawler [1981] Seasonality Index methodology to monthly recharge data). The model simulates karst recharge processes based on the general conceptual model of the soil and the epikarst (Berthelin & Hartmann, 2020; Williams, 1983) incorporating karstic heterogeneity by assuming distributions of subsurface properties such as soil and epikarst storage capacities, or epikarst hydraulic properties. Recharge amount and karst storages are extracted from a 27-year simulation period (1992–2019) driven by daily precipitation and temperature (Rodell et al., 2004), and potential evaporation (Priestley-Taylor-Equation, Martens et al., 2017; Miralles et al., 2011) applied over a $0.25° \times 0.25°$ grid globally over all karst regions. Simulation uncertainty is obtained by running the model 250 times over the entire period and simulation area using randomized parameter values resulting in realistic simulations at monthly time scales (Hartmann et al., 2020).

2.2. Geostatistical Analyses

To advance our understanding on the ideal conditions for a climate signal to be preserved in speleothem annual growth rate records, and inform their role in geochronological applications, a geostatistical approach was used to elucidate common properties and potential climatic, hydrological, and environmental forcing.

Basic descriptive statistics (mean, standard deviation) were calculated for the lamina thickness (the one-dimensional annual extension or growth rate) data as well as the duration of laminated growth sequences. For speleothems with multiple laminated growth phases, statistical analyses were undertaken on each laminated growth phase.

Geostatistical analyses were undertaken on the speleothem lamina time series (growth rate, duration of laminated growth), and results were compared to associated speleothem and/or cave meta-data.

We applied variogram analysis of laminae times series to characterize the behavior of these temporally correlated data, following Mariethoz et al. (2012). The resulting parameters are described in Glossary (Range, Sill, Nugget, and Information Content). These indicators were determined for each time series longer than 50 years ($n = 56$). In addition, the flickering of growth rate (f; see Glossary), which is the lag-one correlation of the acceleration of annual growth rate, was determined following Mariethoz et al. (2012). Flickering has been proposed to occur as a consequence of the presence of karst water storage (Mariethoz et al., 2012). We computed the variability of each of the above metrics across all sites, and compared it to the variability within each stalagmite, when a stalagmite is composed of many parts separated by hiatuses.

To determine whether step changes in either the mean or variance occur in speleothem annual growth rate time series, we undertook changepoint analysis using the Pruned Exact Linear Time (PELT) method (Killick et al., 2012; see Glossary). Changepoint analysis provides quantified information on the linearity of deposition and the possibility of nonlinear growth rate responses to climate and environmental forcing. Growth rate times series were log-transformed to normalize the data prior to changepoint analysis on the mean. The time series were LOWESS detrended using a 0.1 span before changepoint analysis of variance. During PELT changepoint analysis, the minimum segment length was defined as 1 year, the assumed test statistic was normal, and the Schwarz Information Criteria penalty was applied. The *R* package "changepoint" was implemented through Microcal Origin.

We applied spectral analysis on annual growth rate time series longer than 300 years to investigate the strength of different frequency components using the Redfit software (Schulz & Mudelsee, 2002; see Glossary). This software enabled the comparison of speleothem growth rate time series to a first-order

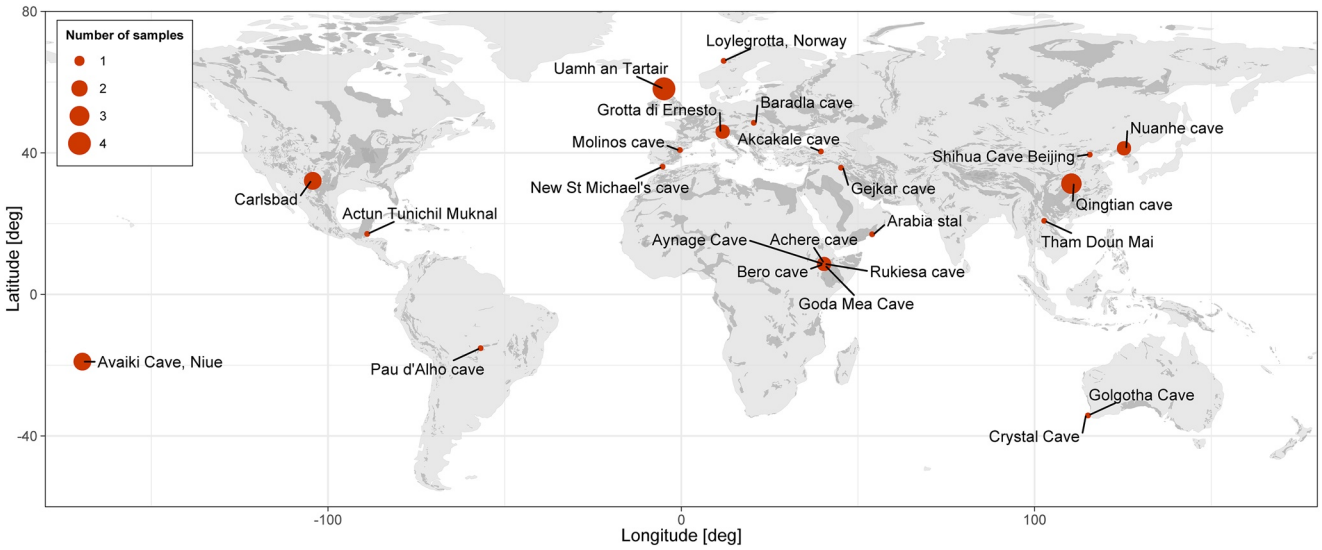

Figure 2. Map showing locations of laminated stalagmites investigated here. Gray shaded areas are the global karst extent (Goldscheider et al., 2020).

autoregressive (AR1) red noise background. This allows the identification of the frequencies (time periods) that stalagmite growth rate time series statistically different from red noise, and potentially contain climate information. For all series, a Blackman-Harris data window was used on data which had been segmented every 200 years of laminated record. Spectral peaks were recorded for cases where there were at least 7 "cycles" possible over the duration of laminae.

Age-depth profiles of laminated stalagmites were investigated using standard regression analyses. This allows the investigation of linearity, or otherwise, of stalagmite vertical accumulation. If accumulation rate is close to linear, this benefits geochronological applications.

3. Results and Interpretation

3.1. The Database

We identified 39 laminated speleothem time series, whose geographic positions are shown in Figure 2. Summary information describing the cave metadata is presented in Tables 1 and 2 and time series, presented as growth rate versus time, in Figure 3. The 39 records derived from 23 caves and 6 continents (Figure 2). Stalagmites are the only speleothem type with archived growth rate data, however laminated sequences are present but unarchived in stalactites and flowstones (e.g., Broecker et al., 1960). Twenty-two records were found in the SISAL v2 database (SISAL entities 85–88, 108, 128, 182, 217, 229, 279 (partial record), 382–386, 465, 466, 506, 507, 559, 573, and 672). There are an additional eight records previously analyzed for their growth geostatistics from Mariethoz et al. (2012) and which were predominantly archived in the World Data Centre—Paleoclimate. We add nine additional records, five new records from the WDC Paleoclimate, and four previously unarchived or unpublished records. The annual periodicity of all 39 laminated speleothem time series has been assessed by the original authors through comparison with the most appropriate radiometric dating method for their period of deposition (atmospheric bomb test peaks for modern deposition; uranium-thorium or radiocarbon for samples deposited pre-bomb).

The 39 growth rate time series (archived as supporting information) come from the Holocene except for one Ethiopian record (GM-1, Goda Mea, Ethiopia, that formed during the last interglacial). This likely reflects a bias due to a focus of paleoclimate research to high-resolution climate investigations of the last millennia. Four caves have multiple stalagmite records, including coeval deposition (Uamh and Tartair, UK; Avaiki Cave, Niue; Grotta di Ernesto, Italy and Qingtian Cave, China).

Sixty-four percent of the stalagmites ($n = 25$) have a single laminated growth period reported by the authors; 21% have two growth phases and 15% have more than two growth phases. We suggest that this could include

Reviews of Geophysics

10.1029/2020RG000722

Table 1

Summary Table With Site Description for Each Annually Laminated Stalagmite, With Samples Listed by Geographical Region

Entity name	Entity ID (<1,000 = SISA Lentity ID)	Site name	Lat (°, N is +ve)	Long (°, *E* is +ve)	Altitude (m)	Cover thickness (m)	Mean annual *T* (° C)	Total annual P (mm)	PET (mm)	Aridity Index (P/PET)	Total annual recharge (mm)	Recharge Seasonality Index (RSI)	Precipitation Seasonality Index (PSI)	Geology age	References
Africa															
Ach-3	1013	Achere/Aynage Cave, Ethiopia	8.6	40.4	1,534	30	21	1,294	1,816	0.53	218	0.63	0.55	Jurassic limestone	Not previously published
Ayn-07-5	1018														
Ach-1	229														Asrat et al. (2007)
Merc-1	*87*	Rukiessa cave, Ethiopia			1,618	25									Baker et al. (2007)
Asfa-3	*88*														
Bero-1	*108*	Bero cave, Ethiopia	8.4	40.3	1,363						248			Jurassic limestone and marl	Baker et al. (2010)
GM-1	1014	Goda Mea Cave, Ethiopia	8.5	40.5	1,574	20			1,774	0.56	222	0.61		Jurassic limestone	Asrat et al. (2018)
Europe															
SU967	*85*	Uamh an Tartair, UK	58.1	−4.9	220	10	7.1	1,955	493	2.39	1,479	0.39	0.26	Ordovician dolomite	Baker et al. (2015)
SU032	*86*														
SU961	1007														
SU962	1008														
SU963	1009														
MO-7	217	Molinos Cave, Spain	40.8	−0.4	1,050	20	13.2	434	893	0.60	136	0.40	0.27	Cretaceous limestone	Munoz et al. (2015)
ER76	*279*	Grotta di Ernesto, Italy	46.0	11.7	1,167	20	6.7	1,289	739	1.15	700	0.23	0.34	Jurassic limestone	Scholz et al. (2012)
ER77	*1003*														Frisia et al. (2003)
Gib04a	*182*	New St Michael's Cave, Gibraltar	36.1	−5.3	325	100	18.3	767	1,068	0.69	n.a.	n.a.	0.66	Jurassic dolomitized limestone	Mattey et al. (2008)
NU2	*382*	Baradla Cave, Hungary	48.5	20.5	375	150	9.7	619	837	0.74	357	0.17	0.35	Triassic limestone	Demény et al. (2017)
L-03	1004	Larshullet, Norway	66.0	12.0		60	1.4	1,600	400	5.20	528	0.39	0.25	Metamorphic limestone	Linge et al. (2009)
Middle East															
2p	*559*	Akçakale Cave, Turkey	40.4	39.5	1,530	30	9.9	460	954	0.51	229	0.59	0.33	Jurassic limestone	Jex et al. (2011)

Reviews of Geophysics

10.1029/2020RG000722

Table 1
Continued

Entity name	Entity ID (<1,000 = SISA Lentity ID)	Site name	Lat (°, N is +ve)	Long (°, *E* is +ve)	Altitude (m)	Cover thickness (m)	Mean annual *T* (° C)	Total annual P (mm)	PET (mm)	Aridity Index (P/PET)	Total annual recharge (mm)	Recharge Seasonality Index (RSI)	Precipitation Seasonality Index (PSI)	Geology age	References
Gej-1	*573*	Gejkar Cave, Iraq	35.8	45.2	650	20	13.7	650	1,215	0.62	94	0.75	0.85		Flohr et al. (2017)
S03	1005	Kahf Defore, Oman	17.0	54.0	15–20	20	25.5	74	1,475	0.05	11	0.41	0.62	Eocene limestone	Fleitmann et al. (2004)
China and SE Asia															
QT9	383	Qingtian Cave, China	31.3	110.4	1,630	80	7.4	1,750	924	1.11	506	0.48	0.54	Permian limestone	Liu et al. (2015)
QT24	384														
QT40	385														
QT41	386														
NH6	465	Nuanhe Cave, China	41.3	125.3	500	20	6	850	916	1.07	462	0.81	0.77	Ordovician limestone	Wu et al. (2012)
NH33	466														
TS9501	1006	Shihua Cave, China	39.5	−115.6	251		11.8	577	992	0.59	59	0.59	1.06	Ordovician limestone	Tan et al. (2003)
TM-17	672	Tham Doun Mai, Laos	20.8	102.7	352	180	22	1,200	1,517	1.04	880	0.90	0.86	Silurian limestone	Wang et al. (2019)
North, Central, and South America															
ALHO6	128	Pau d'Alho cave, Brazil	−15.2	−56.8	340		25.5	1,440	1,708	0.83	639	0.85	0.55		Novello et al. (2016)
ATM-7	*507*	Actun Tunichil Muknal,Belize	17.1	−88.9	40	40	25	1,730	1,442	1.20	1,058	0.54	0.47	Cretaceous limestone	Frappier et al. (2007)
BC-11	*506*	Carlsbad Cavern, USA	32.1	−104.3	1,300	30	14	390	1,578	0.20	40	0.44	0.60	Permian dolomite/ limestone	Asmerom et al. (2013)
BC2	1001														Rasmussen et al. (2006)
HC1	1002														
Australasia and Pacific															
ASM1	*1010*	Avaiki Cave, Niue	−19.0	−169.5		20–30	26	2,052	1,256	1.27	n.a.	n.a.	0.27	Partially dolomitized Quaternary limestone	Rasbury & Aharon (2006)
ASM2	*1011*														
ASM3	*1012*														
GL-S4	*1015*	Golgotha Cave, Australia	−34.1	115.1	70	30–40	14.75	1,113	1,033	1.06	229	0.93	0.69	Quaternary aeolianite	New records
CRY-S1	*1016*	Crystal Cave, Australia			100										

Note. All data is from the original reference, except for the following. Potential evapotranspiration (PET) is from the Worldclim database. Total annual recharge is calculated using a karst hydrology model (Hartmann et al., 2020) and is not available (n.a.) for small island locations. The seasonality indices are calculated using monthly precipitation and recharge respectively, following the methodology of Walsh and Lawler (1981). Data gaps are where altitude, cover thickness or geology information was not provided by the authors. Entity ID is the SISAL v2 entity (Comas-Bru, Rehfeld, et al., 2020) where <1,000, and >1,000 for newly defined entities. Entity names and IDs in italics are samples that were still depositing when sampled.

Table 2
Geostatistical Summary, With Samples Sited by Entity ID

					Variogram properties					Changepoint analysis		
Entity ID	Entity name	Lamina type	Total laminae (*n*)	Lamina phases (*n*)	Range *r* (years)	Sill *c*	Nuggetn	Information Content (IC)	Flickering (*f*)	Number of changepoints (mean)	Number of changepoints (variance)	Years between variance changepoints
85	SU967	FOM	1,090	1	68.8	0.44	0.18	0.71	−0.31	1	5	218
86	SU032	FOM	326	1	32.3	0.64	0.30	0.68	−0.46	0	5	65
87	Merc-1	Fabric	111	1	6.8	0.52	0.23	0.69	−0.42	0	0	
88	Asfa-3	Fabric	107	1	11.8	0.67	0.19	0.78	−0.33	0	0	
108	Bero-1	Fabric	989	6	117.3	0.75	0.31	0.70	−0.53	0	6	165
128	ALHO6	Fabric	1,496	1	254.3	0.57	0.34	0.62	−0.44	1	3	499
217	MO-7	Fabric	4,094	2	79.0	0.49	0.30	0.62	−0.34	2	15	273
229	Ach-1	Fabric	448	1	42.9	0.45	0.53	0.46	−0.42	0	0	
279	ER76	Fabric, FOM POM	549	4	50.0	0.68	0.13	0.75	−0.33	0	0	
182	Gib04a	Fabric	56	1						0	0	
383	QT9	Fabric, FOM	1,005	1	255.8	0.32	0.28	0.53	−0.38	0	3	335
384	QT24	Fabric, FOM	593	1	87.0	0.41	0.11	0.79	−0.35	0	4	148
385	QT40	Fabric, FOM	903	1	232.7	0.72	0.10	0.88	−0.26	1	11	82
386	QT41	Fabric, FOM	816	1	318.5	0.83	0.39	0.68	−0.27	0	2	408
382	NU2	Fabric	146	1	39.3	0.35	0.45	0.44	−0.32	0	1	
465	NH6	Fabric	980	1	24.2	0.16	0.12	0.57	−0.27	1	10	98
466	NH33	Fabric	883	1	109.1	0.43	0.24	0.65	−0.32	1	4	221
506	BC-11	Fabric	1,399	1	368.2	0.24	0.80	0.23	−0.41	0	2	700
507	ATM-7	Fabric	25	1						0	0	
559	2p	Fabric	258	2	28.8	0.70	0.28	0.71	−0.41	0	3	86
573	Gej-1	Fabric	1,850	2	72.3	0.40	0.60	0.40	−0.32	0	7	264
672	TM-17	Sr	1,933	1	129.9	0.73	0.30	0.71	0.07	0	6	322
1001	BC2	Fabric	2,482	2	223.7	0.39	0.53	0.42	−0.41	0	3	827
1,002	HC1	Fabric	2,062	3	140.2	0.33	0.44	0.44	−0.41	0	3	687
1003	ER77	Fabric, FOM, POM	462	2	189.2	0.26	0.25	0.61	−0.27	1	2	231
1004	L-03	FOM	2,782	1	87.7	0.40	0.26	0.60	−0.35	1	26	107
1005	S03	Fabric	777	1	23.4	0.53	0.38	0.58	−0.35	0	0	
1006	TS9501	Fabric	2,659	1	238.8	0.57	0.48	0.54	−0.39	2	11	242
1007	SU961	FOM	1,874	2	49.5	0.46	0.18	0.71	−0.39	2	9	208
1008	SU962	FOM	1,454	3	157.3	0.75	0.12	0.84	−0.36	1	15	97
1009	SU963	FOM	1,780	2	167.6	0.75	0.18	0.81	−0.40	1	11	162
1010	ASM1	Fabric	172	1	67.1	0.39	0.69	0.36	−0.37	0	1	
1011	ASM2	Fabric	224	1	104.9	0.82	0.53	0.61	−0.33	0	1	
1012	ASM3	Fabric	127	1	4.5	0.44	0.61	0.42	−0.40	0	1	
1013	Ach-3	Fabric	921	4	17.8	0.52	0.34	0.60	−0.33	0	7	132
1014	GM-1	Fabric	1,352	4	17.0	0.56	0.36	0.61	−0.33	0	7	193
1015	GL-S4	Sr	845	1	281.6	0.51	0.47	0.52	−0.40	0	3	282

Table 2
Continued

Entity ID	Entity name	Lamina type	Total laminae (*n*)	Lamina phases (*n*)	Variogram properties: Range *r* (years)	Sill *c*	Nuggetn	Information Content (IC)	Flickering (*f*)	Changepoint analysis: Number of changepoints (mean)	Number of changepoints (variance)	Years between variance changepoints
1016	CRY-S1	Sr	51	1						0	1	
1018	Ayn-07-5	Fabric	178	2	16.7	0.58	0.23	0.72	−0.31	0	0	

Note. Entity ID is the SISAL v2 entity (Comas-Bru, Atsawawaranunt, et al., 2020; Comas-Bru, Rehfeld, et al., 2020) where <1,000. Lamina type abbreviations: FOM, fluorescent organic matter; POM, particulate organic matter; Sr, strontium. For samples with <100 total laminae, variogram analysis was not possible. Entity IDs in italics are samples that were still depositing when sampled.

a sampling bias as researchers focus on the "best" (most continuously laminated) samples. Samples from Ethiopia are notable in having multiple laminated growth phases (with Bero-1 being the sample with most phases, 6).

Eighteen stalagmite laminae series were from samples known to have been actively growing when collected, and the observed growth duration is therefore a minimum. We note that the reported growth duration may also be a minimum if analyses were made over a specific period of interest. Twenty-one stalagmite laminae series had lamina sequences that terminated "naturally," for example, there was a growth hiatus at the top of a lamina sequence.

Lamina type was predominantly reported as changes in calcite fabric ($n = 24$). We note that visible laminae are often described as due to calcite fabric variations, but our experience is that with further investigation by scanning electron microscopy these laminae may relate to sorption of particulate or colloidal organic matter, with or without changes in their fabric. Five samples from the Chinese monsoon region (Shuihua Cave and Qingtian Cave) had both fluorescent and fabric laminae. Six stalagmites from two caves with overlying peaty soils had laminae preserved through annual fluorescence intensity variations (Uamh an Tartair, UK; Larshullet, Norway). One stalagmite from Laos (Tham Doun Mai) and two stalagmites from Western Australia (Crystal Cave, Golgotha Cave) had annual Sr variations identified from synchrotron-light generated micro X-Ray Fluorescence two-dimensional mapping of trace element variability distribution.

Laminated stalagmites have been reported from a wide range of host rock geological ages (from Ordovician to the present-day) and lithologies (limestone, dolomite and aeolianites). Despite the intuitive perception that geological age of the karst rock will influence the karst hydrology, with decreasing primary porosity in older carbonates, and that the lithology would likely affect stalagmite trace element composition, any relationship between lamina type and geological age or lithology is hard to determine. For example, annual Sr laminae are observed in stalagmites from caves developed in Late Quaternary aeolianite (Crystal Cave and Golgotha Cave, Australia), Silurian limestone (Tham Doun Mai, Laos) and Ordovician dolomitic limestone (unarchived data from Uamh an Tartair, UK, Roberts et al., 1998). In our data set, laminae comprised of particulate matter and fluorescent organic matter are only observed in relatively old limestone or dolomite lithologies (Permian limestone at Qingtian Cave, China; Jurassic limestone at Grotta di Ernesto, Italy; Ordovician dolomitic limestone at Uamh an Tartair, UK; and Scandinavian Caledonide metamorphic limestone at Larshullet, Norway). A larger data set is needed to determine if Sr laminae types are due to the dominance of fracture-flow in the older limestones and marbles and very high porosity in the more recent aeolianites and if particulate laminae are related to the porosity inherent to old dolomitized/metamorphosed limestones.

Laminated stalagmites have been reported from between 35°S and 66°N (Figure 2). The metadata for each site is presented in Table 1, and selected modern hydroclimate and cave parameters are visualized as boxplots in Figure 4. Climate parameters are for the modern climate, as reported by the authors. Annually laminated stalagmites have been reported from locations with a wide range of MAT (1.4°C–26°C, Figure 4a) and total annual precipitation (74–2,052 mm, Figure 4b). The precipitation seasonality index (PSI) ranges from 0.25 to 1.06 (Figure 4c). Walsh and Lawler (1981) defined values of PSI < 0.19 as locations where

precipitation is spread through the year, and no laminated stalagmites have been reported for sites with no precipitation seasonality. Laminated stalagmites are predominantly found where precipitation has a definite wetter season (PSI: 0.20–0.39) (37% of stalagmites); is seasonal with a short dry season (PSI: 0.40–0.59; 34% of stalagmites) or seasonal (PSI: 0.60–0.79; 21% of stalagmites). Samples have only rarely been reported at locations with a long dry season (PSI: 0.80–0.99; 5% of stalagmites) or with precipitation < 3 months (PSI: 1.00–1.19; 3% of stalagmites).

Laminated stalagmites have been analyzed from caves with a wide range of annual PET of between 400 and 1,816 mm (Figure 4d), which reflects the wide range of latitudes and MAT of the sites. The resulting Aridity Index (AI), the ratio P/PET, is log-normally distributed (Figure 4e), with most laminated stalagmites found at sites with an AI < 1.27, and an interquartile range of 0.53–1.20. Laminated stalagmites have been rarely analyzed from semiarid (AI < 0.5) environments. We interpret this to be due to insufficient water availability for continuous stalagmite deposition. Laminated stalagmites are also rarely analyzed from environments with significant annual water excess (AI > 2), which we interpret as due to limited seasonality of recharge.

We compare the sites with laminated stalagmites to modeled recharge for the site. We also derive a "Recharge Seasonality Index," using the modeled mean monthly recharge amounts to determine a seasonality index, using the same methodology as applied to monthly precipitation by Walsh and Lawler (1981). We observe that laminated stalagmites have been reported over a wide range of total annual recharge, from 11 mm/year (Kahf Defore, Oman) to 1,479 mm/year (Uamh an Tartair, UK). Laminated stalagmites from caves with recharge <100 mm/year are found also at Carlsbad Cave (USA), Shihua Cave (China), and Gejkar Cave (Iraq). Given the continuous deposition of stalagmites for hundreds or thousands of years at these caves, this suggests that a substantial subsurface focusing of recharge is occurring to enable sufficient water supply, including that from infrequent high-rainfall amount events. The modeled monthly mean recharge for each cave site is presented in Figure S2, together with the Recharge Seasonality Index. The Recharge Seasonality Index ranges from 0.17 (low seasonality, Baradla Cave, Hungary) to 0.93 (strongly seasonal, Golgotha and Crystal Caves, Australia). Stalagmites with hydrologically derived laminae (fluorescent organic matter, colloidal/particulate organic matter and trace elements) are found across the range of seasonal recharge (recharge seasonality index >0.39). Mid-latitude sites with low recharge seasonality and annual fabric laminated stalagmites might be explained by a predominant seasonal cave climate control on calcite fabric. In contrast, mid-latitudes sites with high recharge seasonality could have a dual control on annual lamina formation: the seasonality of cave climate (imprinting the fabric change) and hydrology (determining the amount of vertical extension within that period).

For most stalagmites, data on the cover thickness above the cave is available. Although the cover thickness may not relate closely to the water residence time in the bedrock, the log-normal distribution of the cover thickness data (Figure 4f) suggests that relatively shallow caves (<100 m cover thickness) is where laminated stalagmites are preferentially located (an exception is Tham Doun Mai, Laos, at 180 m cover thickness). Increased water mixing and increasing water residence time with depth likely explains the less frequent observation of laminated stalagmites with depth, although there may also be a sampling bias to researchers focusing on shallow caves.

3.2. Annual Lamina Thickness (Growth Rate) Properties and Metadata Comparison

Figure 5 presents the distribution of all annual growth rates for all 39 speleothems. The distribution follows a log-normal distribution. The mean annual growth rate is 0.163 mm, and the median is 0.093 mm. The slowest annual deposition (10 percentile) is less than 0.018 mm and the fastest (90 percentile) is more than 0.404 mm, with an inter quartile range of 0.200 mm (0.037–0.237 mm). This range of annual growth rate agree with that theoretically predicted by growth rate modeling (Baker et al., 1998). Within the distribution of all annual growth rates, those derived from annual fluorescent laminae alone are the lowest (average = 0.034 mm, median = 0.030 mm), due to location of these samples at cool climate sites (see below).

We compare the annual growth rate data to the modern hydroclimate and geospatial metadata for each site. We use the mean growth rate for each deposition phase, and Holocene speleothems only, assuming negligible change in hydroclimate over the Holocene in comparison to the large range of modern climate covered

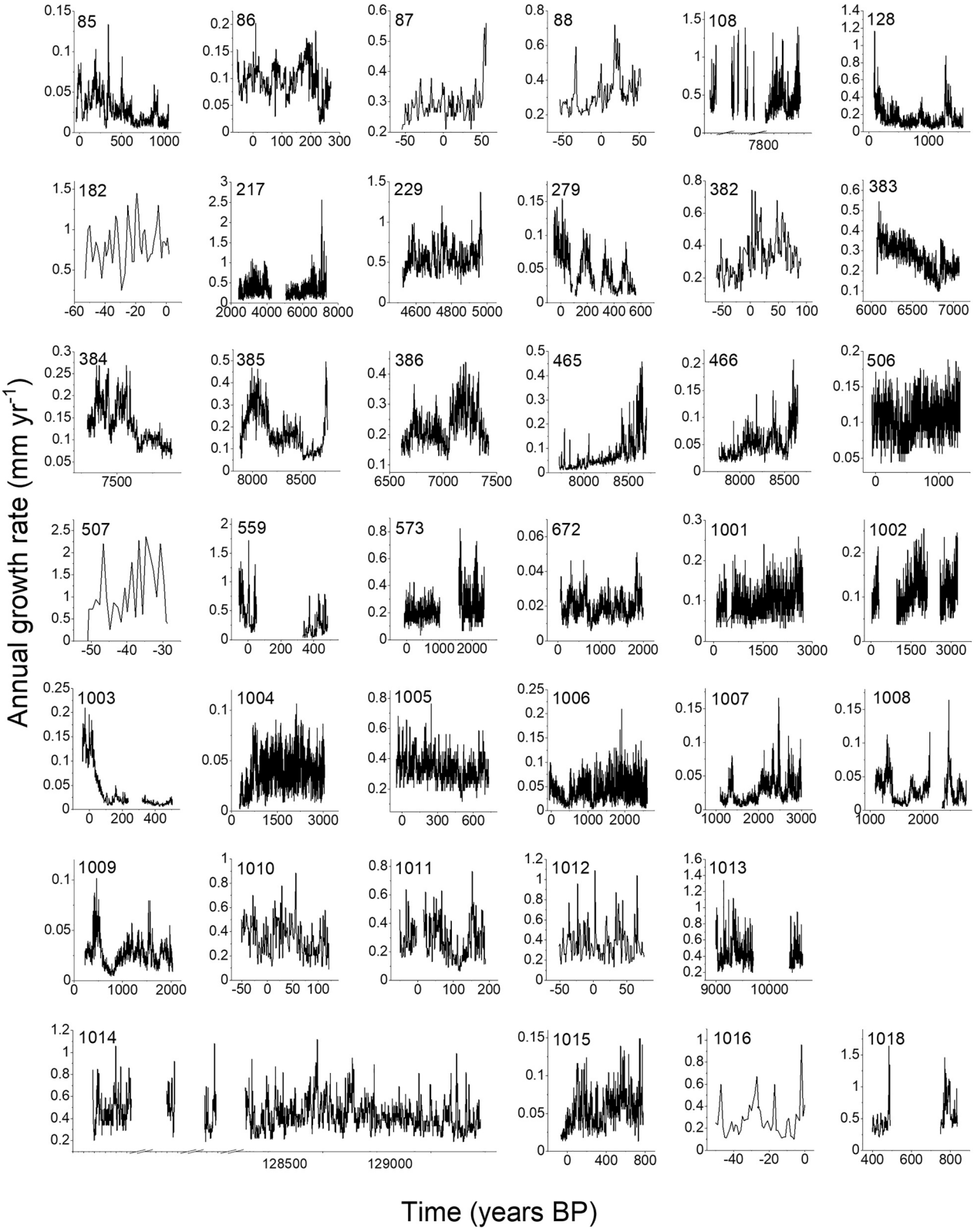

Figure 3. All data presented as time versus annual growth rate. The graph labels show the entity ID as tabulated in Tables 1 and 2. Note different axis scales are used to best visualize individual time series. Years BP refer to years before present where present is 1950 CE.

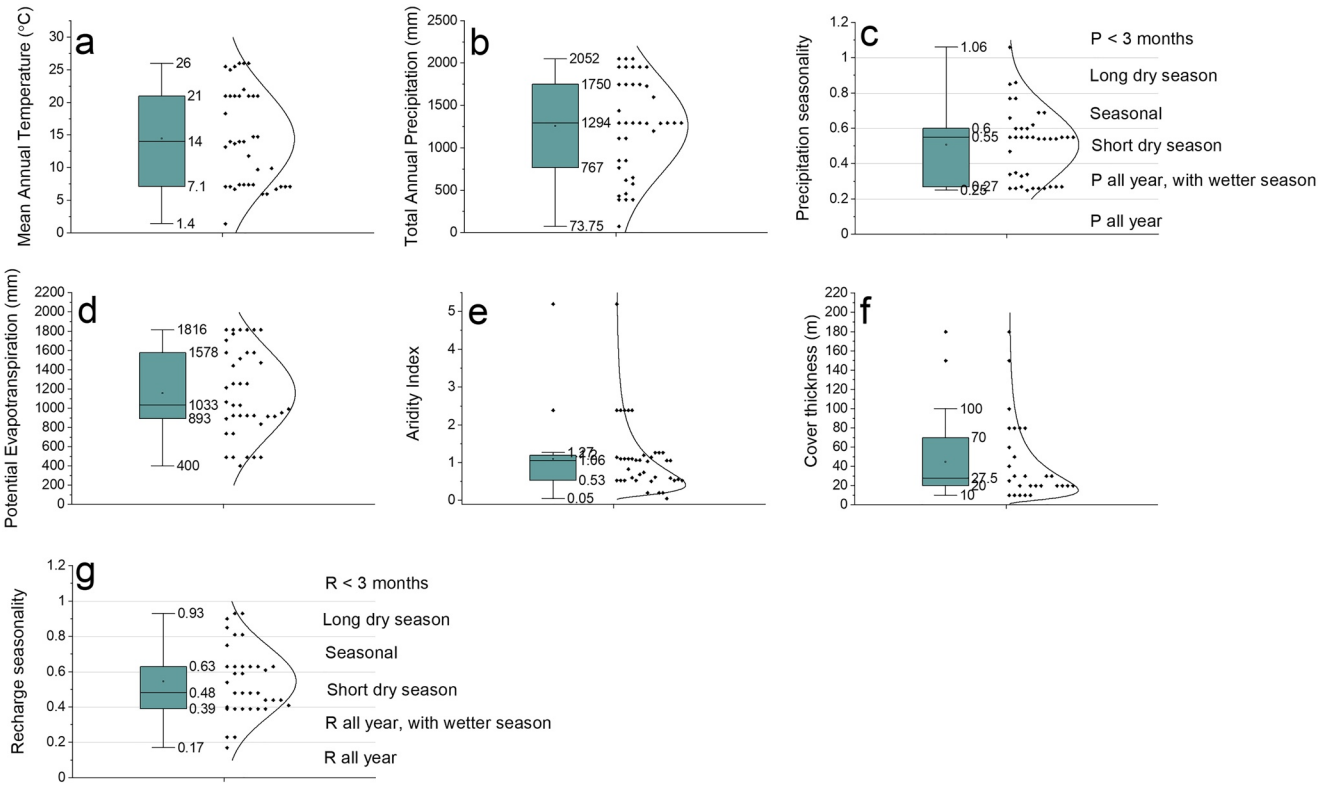

Figure 4. Distributions of hydroclimate and site metadata for annually laminated stalagmites. (a) Mean annual temperature, (b) total annual precipitation, (c) Precipitation Seasonality Index (PSI), (d) potential evapotranspiration, (e) Aridity Index, (f) cover thickness, and (g) Recharge Seasonality Index. Information on data sources are provided in Table 1. The definitions for the PSI are from Walsh and Lawler (1981) and are adopted for recharge seasonality.

by the data set (MAT from 1.4°C to 26°C, total annual precipitation from <100 to 2,052 mm, PET from 400 to 1,816 mm; see Table 1). Using the Spearman's rank correlation coefficient (r_s), we observe a strong, positive correlation between annual growth rate and MAT ($r_s = 0.64$) and PET ($r_s = 0.69$) and negative correlation with latitude ($r_s = -0.64$; all significant at a 99.9% confidence interval, Table S2). These three co-varying hydroclimate parameters represent the warming temperature gradient from pole to equator. The associated increased PET additionally reflects its derivation from T and latitude using the Hargraves methodology (Hargraves et al., 1985). There is no correlation between mean annual growth rate and total annual precipitation ($r_s = -0.07$), negative correlations with modeled average soil and epikarst store fullness ($r_s = -0.50$ and -0.51 respectively) and modeled annual total recharge ($r_s = -0.52$) and a positive relationship with recharge seasonality ($r_s = 0.52$), all correlations significant at a 99.9% confidence interval. These relationships demonstrate the inter-relation of hydrological and climatic controls on growth rate at the global scale, with slow growth rates at sites with high recharge due to the inverse correlation of recharge to PET ($r_s = -0.68$) and MAT ($r_s = -0.59$; both significant at 99.9% confidence interval).

The relationship between growth rate and latitude and MAT is shown in Figure 6, comparing with modern temperatures as reported by the authors (Figure 6b) for all Holocene-aged samples, and for historical CRU TS4.04 gridded temperature data for samples deposited since 1901 CE (Figure 6c). Correlations ($r = 0.40$ for all samples; 0.45 for samples deposited since 1901 CE) are similar for both temperature comparisons. Stalagmites with annual laminae due to changes in calcite fabric and those with fluorescent or trace element laminae are shown in Figure 6b, with laminae from organic matter fluorescence predominantly at cooler climates. The temperature sensitivity of growth rate at the global scale agrees with the theorized primary control on speleothem growth rate of drip water calcium concentration (Buhmann & Dreybrodt, 1985). Soil and vadose zone carbon dioxide productivity is temperature dependent, as demonstrated empirically for global soil PCO_2 (G. A. Brook et al., 1983). This carbon dioxide generates the subsequent dissolution of carbonate and increase in drip water calcium concentration. Global analyses of cave drip waters have shown

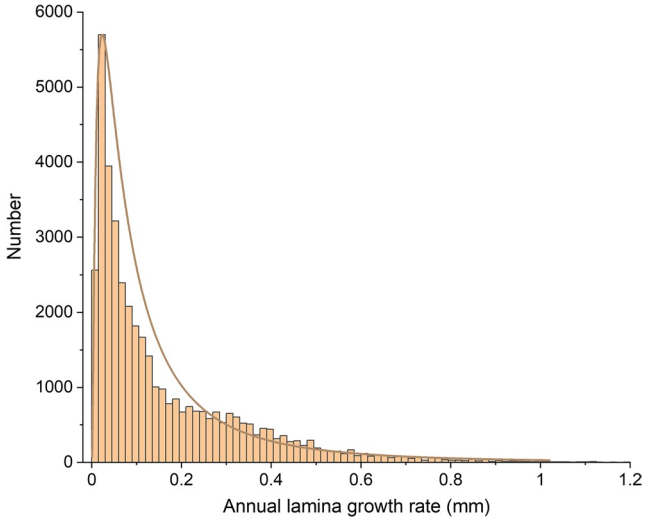

Figure 5. Distribution of annual lamina thicknesses for the stalagmites listed in Table 1. Lognormal curve shown for comparison.

a good agreement with modeled drip water calcium concentration and temperature, using the relationship of G. A. Brook et al. (1983), especially for temperate climates (Baker et al., 2016; Borsato et al., 2015, 2016). One outlying sample with relatively low growth rate, at latitude 20.8°N and 180 m depth, is stalagmite TM-17 from Laos (Wang et al., 2019) with annual Sr laminae. Hydrological data reported for the sample suggested piston-flow hydrological behavior, for example, discrete "parcels" of water movement of similar age and limited mixing. Such a flow path would indicate that carbonate dissolution would be closer to a "closed" system evolution than an "open" system evolution, which could explain the lower growth rate, and the depth of cave further means that substantial PCP is likely to have occurred along the flow path due to the slow percolation through the thick rock burden.

3.3. Duration of Laminated Sequences

The total number of laminae reported in each speleothem sample, and the number of laminated growth phases, are reported in Table 2. We investigate the duration of annual lamina deposition, and its relations to metadata. We note that for stalagmites with multiple laminated growth phases, the intervening period could represent either a growth hiatus (e.g., a period with no dripping, drip water diversion, or dissolution due to drip waters becoming aggressive with respect to calcium carbonate), or a period of deposition without clear lamina formation or a condensed interval where the growth rate is lower than the spatial resolution of the analytical method (typically 2–20 μm), or where concentration of a trace metal falls below the limit of detection of the analytical method. Additionally, many of the samples have been harvested for scientific analysis often concentrated on the last few hundreds or thousands of years, and the duration of laminae deposition is therefore a minimum value (for example, Grotta di Ernesto stalagmite ER76 is laminated in its entire 8,000 years growth, and the complete Laotian TM17 record is almost continuously laminated for about 38,000 years). Finally, we acknowledge there is a possible sampling and research bias, where the most continuously laminated stalagmites were selected.

In stalagmite growth phases that were not terminated by sampling (number of growth phases = 41), we observed a median length of continuous annual laminae deposition of 447 years and an inter quartile range of 177–1,004 years (Figure 4, data presented in Table S1). Laminated sequences of shorter duration are identified in stalagmites from Ethiopia. Treated separately, these have a median duration of 172 years and interquartile range of 69–340 years (Figure 7). Deposition of calcium carbonate in the region has been proposed to be limited by the tectonic activity associated with the East African Rift, which disrupts water flow paths and stores it in the karst (Asrat, 2012, in Fairchild & Baker, 2012). For all sites excluding Ethiopia, the median duration of laminated sequences is 815 years (inter-quartile range of 315–1,668 years; Figure 7).

Outlier samples have unusually long duration lamina sequences and are from cold-climate Larshullet stalagmite L-03 (Norway) and extra-tropical, relatively cool monsoon climate Shihua Cave, China (TS9501). Where there are multiple stalagmites from the same cave or region, we observe a within-site variability that covers the whole range of the data (e.g., Carlsbad Cavern laminated deposition ranges from 266 to 2,167 years). For individual stalagmites, within sample variability in the duration of laminated sequences is also significant, for example, Uamh an Tartair stalagmite SU961 has durations ranging from 206 and 1,668 years, and Carlsbad Cavern stalagmites BC2 and HC1 have durations of 316 and 2,168 years and between 267 to 1,134 years, respectively.

Finally, we compared the duration of continuous lamina deposition against the available metadata using the Spearman's correlation coefficient (Table S3), considering only growth phases not affected by stalagmite harvesting and excluding Ethiopian stalagmites where growth is likely truncated by tectonic processes (remaining samples, $n = 30$). No statistically significant correlations exist ($r < 0.36$, $p > 0.05$).

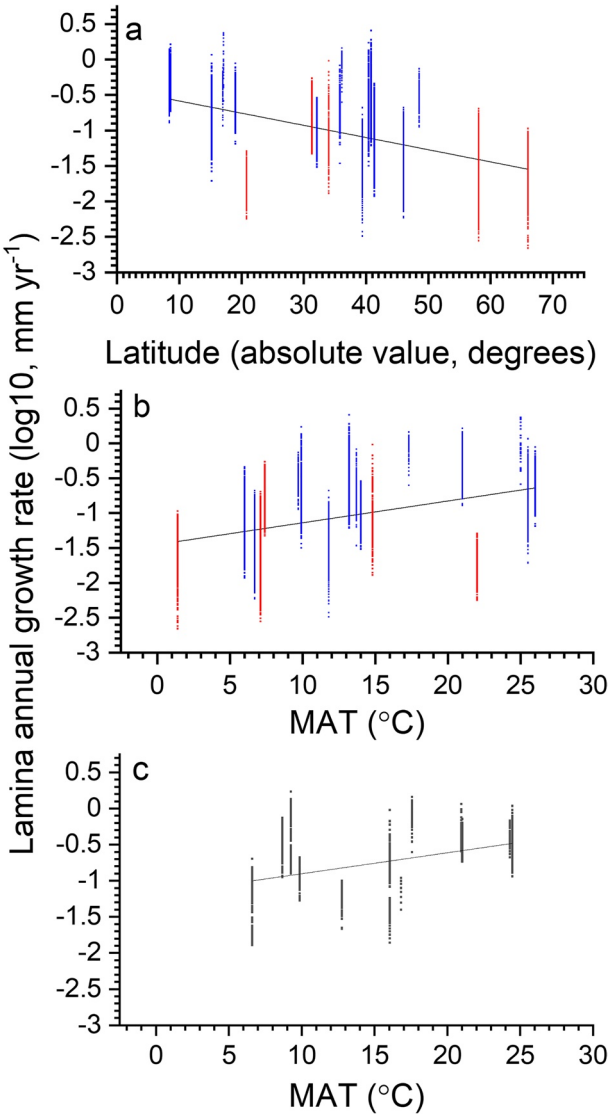

Figure 6. (a) Relationship between lamina thickness and latitude, (b) mean annual temperature (all Holocene samples), (c) mean annual temperature 1901–2019 CE (coeval entities only). In (a) and (b), fabric and particulate organic matter laminated stalagmites are blue and Sr or FOM laminae in red. 1901–2019 CE temperatures are from the Climate Research Unit (CRU) gridded surface temperature 4.04 (Harris et al., 2020).

Overall, our global analysis suggests there is no statistical relationship between lamina duration and hydroclimate, and that within-cave and within-sample variability in lamina duration is as large as the global range. From this, we infer that the duration of laminated deposition is in general controlled by site-specific factors, for example, hydrologically controlled by specific flow paths, and in the case of Ethiopian samples, there is a likely tectonic control. We investigate this further in Section 4, where we characterize laminated stalagmites by all their growth properties, including the duration of continuous lamina deposition.

3.4. Geostatistical Properties of Growth Rate Time Series

3.4.1. Variogram Analysis and Flickering

The variogram properties nugget effect (n), sill contribution (c), information content (IC), range (r), and the flickering parameter (f), were determined for each laminated growth phase. The distribution of IC, r, and f are presented in Table 2 and Figure 8, and the results for individual growth phases in Table S1. A comparison of IC, r, and f between fabric laminated stalagmites and stalagmites with fluorescent organic matter (FOM) and Sr laminae is presented in Figure S2. The nugget and sill are not shown, as the IC represents the relative value of nugget to sill in the variogram.

Figure 8a shows the IC, where a value of 0 is pure noise and 1 a completely smooth autocorrelation function. IC values are normally distributed, with a median IC of 0.65 and an inter quartile range of 0.53–0.71. Outlying IC values come from two stalagmites from Carlsbad Cavern, USA, that show relatively noisy variogram properties. As previously observed for the duration of laminated deposition, there is significant within site variability. For example, four stalagmites from Qingtian Cave, China, have IC between 0.53 and 0.88. There is also substantial within-sample variability. For example, a third Carlsbad Cavern stalagmite has an IC varying between 0.36 and 0.58. Despite this variability, comparison between fabric laminated stalagmites and stalagmites with either FOM or Sr laminae shows the latter group have a higher mean IC (0.73 vs. 0.58). The inter quartile range for IC for stalagmites is 0.46–0.69, and for FOM or Sr laminated stalagmites from 0.66 to 0.81 (Figure S2). The difference in IC between the two groups is significant at a 99% confidence level (Student's t-test). Stalagmites with laminae preserved through FOM or Sr laminae have a less noisy annual growth rate autocorrelation function, which we infer is due to a combination of (1) FOM laminated stalagmites occurring at cooler and wetter sites, where karst stores remain relatively full (see next section) and (2) FOM and Sr laminae are more directly related to the hydrological year, whereas changes in speleothem fabric could be related to both seasonal changes in drip water chemistry lamina and seasonal changes in cave climate. Especially in mid-latitudes, fabric laminated stalagmites could preserve a combination of cave climate year, with ventilation occurring close to the equinoxes, and the hydrological year, potentially introducing additional noise.

Figure 8b shows the variogram range, which is the duration of temporally correlated data, and includes data from all stalagmites. This parameter has a log-normal distribution, with a median of 67 years and an inter quartile range of 23–157 years. The longest range is observed in a stalagmite from Carlsbad Cavern (421 years, stalagmite BC2). All values of variogram range for the caverns are between 21 and 421 years), indicating a significant within sample and between sample variability at a site. Significant within-sample variability is also observed at other sites (for example, stalagmite ER-76 from Grotta di Ernesto (Italy) has

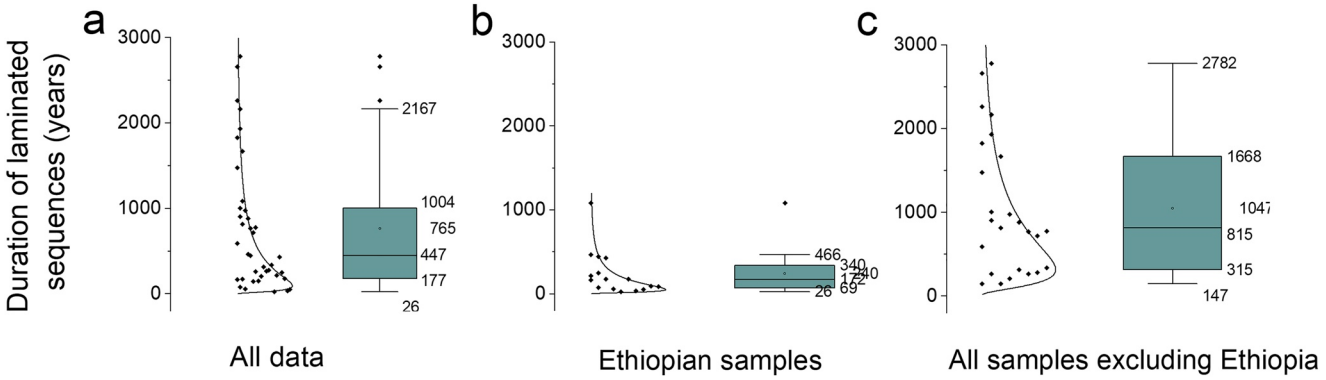

Figure 7. Distribution of duration of laminated stalagmites (a) all data, (b) Ethiopian stalagmites, (c) all data with Ethiopian stalagmites removed.

a range between 6 and 130 years). There is no difference between fabric laminae and other laminae types (Figure S2).

Figure 8c presents the distribution of the flickering parameter f, which can theoretically range from −1 to +1. A value of −0.5 is obtained from white noise and a value of 0 represents no flickering of growth rate increments. Mariethoz et al. (2012) observed flickering in 11 stalagmite growth rate series and interpreted it as due to the damping effect of the stored water volume on inter-annual growth variability. Figure 6c shows the flickering data is normally distributed with outliers exhibiting high and low values of f. The Laotian TM-17 stalagmite has the highest value, $f = 0.07$, indicating it has a very smoothed growth rate time series with no flickering. This concurs with the authors observation of piston-flow hydrology (Wang et al., 2019) and with the interpretation of the flickering phenomena of Mariethoz et al. (2012). The lowest flickering has values lower than the white noise value of −0.5 and occurs in growth phases of the Bero-1 stalagmite from Ethiopia. These f values suggest there is no predictable signal in the inter-annual $(t - 1)$ change in growth rate. The authors report that this stalagmite has bundles of "infiltration laminae" within each year, with occasional seasonal dissolution features (Baker et al., 2010). The intermittent partial dissolution of annual growth would be one explanation for the observed f value. When comparing the flickering of laminae formed from changes in calcite fabric (inter quartile range from −0.33 to −0.51) and those from FOM and Sr laminae (−0.30 to −0.39), there is no statistical difference. We infer that the rate of change of growth rate is dominated by the damping effect of the stored water volume, irrespective of how growth rate is preserved in the stalagmite and how that determines the total annual growth.

Table S4 presents the Spearman's correlation coefficients of the geostatistical parameters with metadata for all laminated growth sequences, including the duration of laminated sequences for samples and average annual growth rate ($n = 55$).

(a) Statistically significant correlations between the nugget and IC ($r_s = -0.83$, 99.9% CI) and sill and IC ($r_s = 0.63$, 99% CI). This is due to the derivation of IC from the ratio of nugget (n) and sill (c)
(b) The nugget correlates with modeled recharge ($r_s = -0.64$, Figure S3a), modeled soil store and epikarst store fullness (both $r_s = -0.66$), MAT ($r_s = 0.57$, Figure S3b), PET ($r_s = 0.45$) and AI ($r_s = -0.43$). These

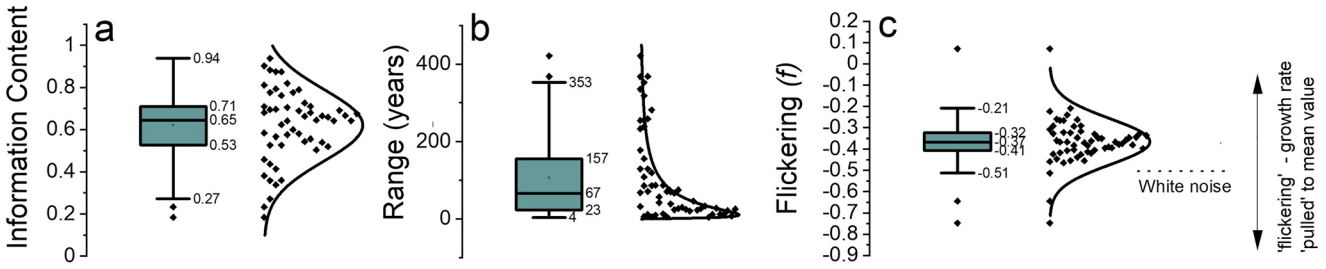

Figure 8. Distribution of geostatistical parameters (a) Information Content (IC), (b) range, and (c) flickering (f).

correlations suggest that decreasing water availability and decreasing recharge leads to a decrease in the water volume in the karst stores supplying stalagmites in warmer climates and could lead to increased nonlinear time series behavior and short-term fluctuations as stores drain and refill

(c) Increasing stored water with increasing recharge would explain the relationship between information content (IC) and modeled soil and epikarst store fullness ($r_s = 0.52$ and $r_s = 0.57$) and modeled recharge ($r_s = 0.54$, Figure S3c)

(d) The flickering parameter f has no significant correlations with any of the site metadata, agreeing with the inference that it relates to the effect of changes in water storage to a specific drip (and therefore sample)

For samples where there are multiple laminated growth phases, we consider the within-stalagmite variability of each geostatistical parameter to its variability across all growth phases. We observe a high within-stalagmite variability, as summarized in Table 3. The increase in standard deviation of a geostatistical parameter from within-stalagmite to all laminated growth sequences ranges from x1.15 (sill) to x1.66 (nugget and flickering). The overall dominance of within-site variability provides evidence for the importance of site-specific and drip-specific control on variogram properties and flickering. When considering all laminated growth sequences, the greater variability in the nugget agrees with the observed global correlations with MAT, recharge, and AI (Figure S3c).

3.4.2. Spectral Analysis and Comparison to AR1 Red Noise

Results of the spectral analyses undertaken on stalagmite laminae sequences longer than 200 years are shown in Figure 9. In general, the spectral properties of stalagmite growth rate time series are indistinguishable from a red noise AR1 process at a 99% confidence level. Stalagmite growth rate times series are fitted to AR1 functions with a median value for the autocorrelation parameter τ, of 2.18 (range 0.91–6.16) years. A higher value of τ indicates a stronger "memory" of previous year's growth rate, and we observe τ values much smaller than the variogram range (i.e., the duration of autocorrelation in growth rate). Table S5 presents values of τ and Spearman's correlation coefficients of τ with metadata for all laminated growth sequences longer than 200 years ($n = 40$). τ most strongly correlates with modeled annual recharge ($r_s = 0.73$), modeled soil and epikarst store fullness ($r_s = 0.72$) and the variogram information content ($r_s = 0.77$), and has no correlation with the duration of autocorrelation in growth rate, the variogram range ($r_s = 0.24$). An autocorrelation with stronger "memory" in stalagmite growth rate time series is more likely when recharge is greater, resulting in fuller soil and epikarst stores, and less noisy variogram properties.

Figure 9 shows that the Laotian TM-17 (entity 672) has a distinctly different spectra from all other stalagmites, with lower spectral power at less than 3-years frequency. Combined with the lack of flickering of growth and relatively slow growth rate for this sample, its spectrum provides additional confirmation of the dominance of piston-flow, with discrete parcels of water feeding the stalagmite.

Spectral analysis of the stalagmite growth rate time series demonstrates that, in general, stalagmite growth approximates an AR1 or red noise signal. This is due to the mixing of recharge waters prior to reaching the cave; tritium dating evidence suggests this a mean water residence time from ~2 to 36 years to decades is possible for caves <50 m below land surface (Jean-Baptiste et al., 2019; Kaufmann et al., 2003; Kluge et al., 2010). However, Figure 9 shows that most stalagmites have some spectral peaks that do exceed the 95% confidence level of a red noise process. Most (88.6%) of these spectral peaks occur at less than 6-year periodicity; with only 11.4% occurring over periods longer than 6 years. This also agrees with the likely water residence time, and associated mixing, between the surface and the cave.

Figure 9 shows that there are no within-site or regional trends for the spectral peaks that are significant compared to red noise. However, the Niue stalagmites, whose growth duration were too short to include in our analysis, do have consistent spectral signals in stalagmite growth rate time series from this ENSO dominated climate region (Rasbury & Aharon, 2006). We interpret the observation of spectral power that is significant compared to an AR1 processes at less than 6-year time periods in this data set as representing the time-window where it is most possible for climate or environmental processes to imprint a signature on growth rate. This would require stalagmites with a suitable hydrological connectivity (less water mixing and mean residence time, resulting in a relatively small growth rate "memory" or τ), as well as sufficiently large climate or environmental variability in a stalagmite growth rate determining process.

Table 3
Within-Stalagmite and Between-Site Variability in Stalagmite Geostatistics

	Range (r)	Sill (c)	Nugget (n)	Information content (IC)	Flickering (f)
Average 1 SD, all laminated growth phases	117.0	0.246	0.180	0.176	0.100
Average 1 SD, within individual stalagmites	83.4	0.214	0.109	0.136	0.061
Average 1 SD within individual stalagmites (weighted)	89.5	0.179	0.111	0.130	0.050
Increase in SD (within-stalagmite vs. all laminated growth phases)	1.40	1.15	1.66	1.29	1.66

Note. The weighted average weights for the total number of laminae within a stalagmite.

Our experiences of climate-sensitive growth rate time series at Grotta di Ernesto and Uamh an Tartair further suggests that sites close to the climatic limit of speleothem formation (cf. Borsato et al., 2016) might yield the strongest climate sensitivity. Both sites are close to such a limit: cool temperatures limiting drip water calcite saturation at Grotta di Ernesto and a soil saturation controlling drip water saturation at Uamh an Tartair. In this regard, sampling stalagmites growing "close to the edge" of their possible range could

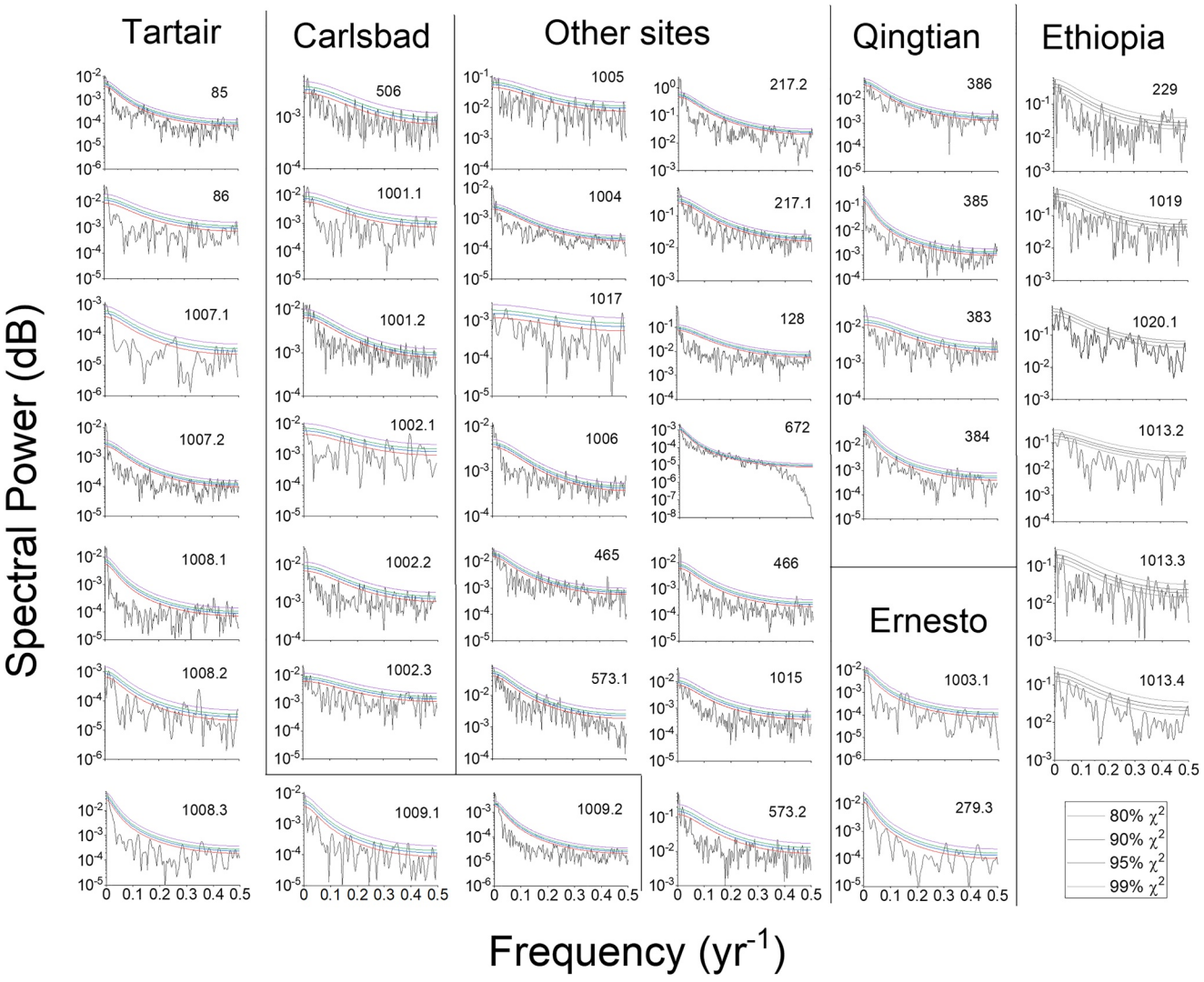

Figure 9. Spectral analyses of growth rate time series for each group phase, compared to AR1 spectra. 80%, 90%, 95%, and 99% confidence intervals for the AR1 spectra are shown. For all graphs, *x*-axis is frequency (1/years) and *y*-axis spectral power in dB. Entity IDs are shown: the suffix refers to the number of the growth phase. For more information on the stalagmite metadata see Tables 1, 2, and S1, and for values of the autocorrelation function τ see Table S5.

amplify their environmental sensitivity, and would be similar to the approach used in dendroclimatology of sampling stressed and climatically sensitive trees, such as close to the treeline. In regions where a multi-year climate driver occurs in the less-than 6-year time frame, such as ENSO, sample replication would ensure the identification of a spectral signature derived from climate forcing rather than it being a function of karst hydrological conditions.

3.4.3. Changepoint Analysis

Results of the changepoint analysis on both the mean and variance of annual lamina thickness time series are summarized in Table 2. PELT changepoint analysis shows there are fewer changes in mean growth rate compared to growth rate variance. Most stalagmites have no changepoints in mean growth rate, and no samples have more than two changepoints. Time series of stalagmites with changepoints in mean growth rate are presented in Figure 10.

Changepoints in mean growth rate operate equally in both directions (e.g., to faster or slower growth). Fifteen changepoints in mean growth rate are observed in 12 of the 39 stalagmites. They are observed at sites where laminae are preserved as FOM (five out of six stalagmites which laminae are uniquely reported as FOM; Larshullet, Norway, and Uamh an Tartair, UK). Other samples with mean growth rate changepoints include four of seven from the Chinese monsoon region (Qingtian Cave, Nuanhe Cave, Shihua Cave), and stalagmites from Grotta di Ernesto (Italy), Molinos Cave (Spain), and Pau d'Alho Cave (Brazil). For these 12 stalagmites, the average duration of laminated growth sequences is 1,462 years (median: 1,444 years), in the upper quartile of duration of laminated stalagmite deposition.

Changepoints in mean growth rate in laminated stalagmites are therefore infrequent. The primary control on growth rate is drip water supersaturation with respect to calcite, which is determined by the extent of soil and vadose zone carbon dioxide productivity. Changes in mean growth rate could represent rapid or non-linear changes on processes that control soil and vadose zone carbon dioxide production, such as wildfire or, in the Anthropocene, land clearance or urbanization. Alternatively, a changepoint could occur due to a permanent flow switching between water stores which have waters of contrasting calcite supersaturation, such as what might occur due to seismic activity or climate change. Another process that can determine growth rate and change rapidly is an alteration in cave ventilation, potentially caused by cave collapse or rapid external temperature change, leading to a significant change in cave air carbon dioxide concentration.

In contrast to the changepoints in mean growth rate, there are more growth rate variance changepoints per sample. Data is summarized in Table 2 and all variance changepoints are presented in Table S6, with selected examples shown in Figure S4. Thirty-one out of the 39 stalagmites have one or more variance changepoints. Six of the seven samples with no variance changepoints have a relatively short duration of laminated deposition of less than 550 years. Overall, there are 189 variance changepoints occurring on average every 213 years (see Figure S4a for an example from Molinos Cave). Two stalagmites from Carlsbad Cavern, USA (Figures S4b and S4c), have the longest interval between changepoints (>680 years), and stalagmite S-03 from Oman has no changepoints over 1,454 years of deposition. These sites have the lowest aridity index observed in the data set (AI < 0.2), suggesting that a very stable supply of stored water is required for continuous laminated stalagmite deposition to occur. The maximum number of changepoints is 26, from stalagmite L03 from Larsullet, Norway (Figure S4d). This is the only stalagmite which preserves both spring (snow-melt flush) and autumn FOM laminae. Variance changepoints are grouped through time, more likely occurring where the authors report multiple laminae per year and relatively warm summer climate (Linge et al., 2009).

Some caves and regions have co-eval stalagmites, allowing investigation of a common control on variance changepoints. At Uamh an Tartair, UK, five stalagmites have periods of coeval deposition. A total of 45 changepoints are observed, occurring between every 65 years to every 276 years, depending on stalagmite. Only 12 variance changepoints could have occurred at the same time (allowing for chronological uncertainties, within ±25 years). Ten of those relate to stalagmites SU961 and SU962 which grew a few cm apart and for which flow switching between stalagmites had previously been reported by the authors (Proctor et al., 2002). For these two stalagmites, there were an additional 14 changepoints which were not coeval. At Qingtian Cave, China, (Liu et al., 2015), overlap of stalagmites chronology between ~7.5 and ~6.5 ka had no coeval variance changepoints, and a frequency of changepoints varying from 82 to 408 years. Changepoints

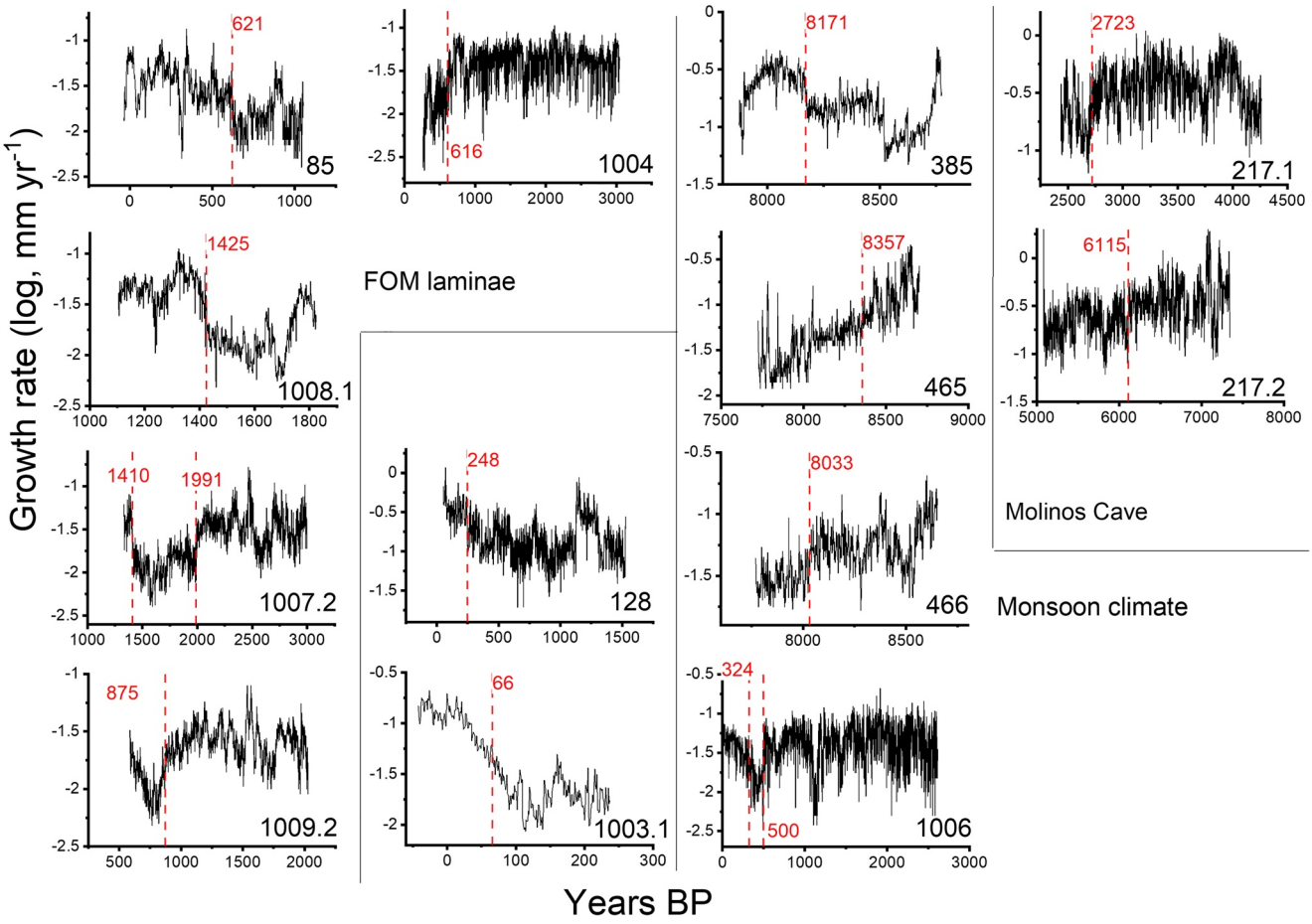

Figure 10. Changepoints in mean growth rate. For all graphs, *x*-axis is years before present, where 0 is 1950 CE, *y*-axis is the log growth rate. Changepoint years BP are shown in red. Entity IDs are shown, for more details see Tables 1 and 2. Entities are grouped by lamina type, climate, or cave where appropriate.

were not coeval for three overlapping stalagmites from Niue, and two coeval stalagmites from Nuanhe Cave, China (Wu et al., 2012).

Overall, variance changepoints occur more frequently than mean changepoints. Where there are coeval stalagmites at a site, there are almost no synchronous variance changepoints. Variance changepoints appear to be largely sample-specific in their timing and frequency, which suggests a lack of common forcing. Therefore, we propose a drip-specific karst hydrology control on growth rate variance, generated by the non-linear nature of karst hydrology due to movement of water stored in one or more voids or fractures and often complex flow paths.

3.4.4. Age-Depth Relationships in Laminated Stalagmites

Given the importance of annually laminated stalagmites in providing geochronological control for other geochemical proxy data, we investigate the age-depth relationships for all stalagmite samples (Figure 11). As might be anticipated from the infrequent occurrence of changepoints in mean growth rate, Figure 11 shows that all stalagmites approximate to a linear age-depth relationship, irrespective of length of deposition or whether samples were sampled whilst still activity forming or not.

We determined the strength of this linear age-depth relationship through regression analysis of all growth phases. For all growth phases, the mean R^2 was 0.98, with 2σ of 0.05. We find no relationship with the duration of laminated sequences from 27 to 2,785 years ($R^2 = -0.01$). The outlying growth phases with relative

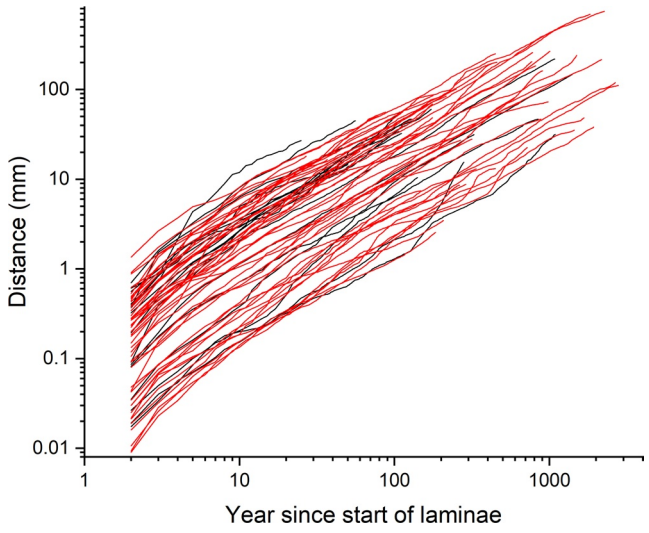

Figure 11. Age versus distance for all samples. Coloring distinguishes samples where lamina formation was ongoing when harvested (black) versus other samples (red). All years and distances are from the start of a laminae growth phase, for example, oldest is bottom-left, end of growth phase (or harvesting) is upper-right. Log-log scale is used to enable the visualization of all age-depth relationships over 2 orders of magnitude vertical extension.

low age-depth linearity are from stalagmites from Grotta di Ernesto, Italy (ER77, 1003.1), Akçakale Cave, Turkey (2p, 559.1), Uamh an Tartair, UK (SU962, 1008.1, and 1008.3) and Qingtian Cave, China (QT40, 385). With the exception of ER77, these are samples with the most frequent changepoints in growth rate variance (SU962 every 97 years; 2p every 86 years; QT40 every 82 years), suggesting that a change in variance in these samples is associated with a change in growth rate that does not result in a changepoint in mean being detected. For most growth phases (92% of all growth phases), the age-depth relationship is linear, with an $R^2 > 0.97$. The strong linear growth over deposition periods from decades to millennia is interpreted as due to the buffering effect of a well-mixed karst water store necessary to ensure continuous stalagmite deposition.

4. Discussion

4.1. Characterizing Laminated Stalagmites

To account for all the statistical and climatic characteristics of the samples, we conduct a multidimensional scaling (MDS) analysis (see Glossary). It consists in a representation of the samples in a high-dimensional space where the "distance" between any pair of samples is given by their dissimilarity in terms of the various criteria considered (Jex et al., 2012). Here the variables considered are: growth rate, the variogram parameters (Range r, Sill c, Nugget n, and Information Content IC), flickering, MAT, total annual precipitation, PET, AI, PSI, modeled recharge, modeled soil and epikarst store percentage fullness, and the Recharge Seasonality Index, resulting in a 15-dimensional space. The autocorrelation parameter τ is not included as this was only available for the subset of samples with growth duration long enough for spectral analysis. The distance chosen is the standardized Euclidean distance. A high-dimensional representation is often needed to map all samples with their correct distances; however, it is often possible to project this space in two dimensions to have an acceptable graphical representation.

This is the case in Figure 12, where the two dimensions illustrated (out of 15 dimensions in total) represent 60% of the information about the pairwise distances among the objects (laminated stalagmite growth phases). Each dot represents a growth phase, and similar growth phases are closer to each other. We only include stalagmite growth phases that were not truncated by sampling. In MDS, the axes cannot be interpreted in terms of the variables used as input, because the projection of a high dimensional space in a 2-D representation results in axes representing many variables at once. The axes are therefore usually not labeled in MDS. However, to facilitate the interpretation, we have performed a k-means classification of the 43 samples using all 15 dimensions, with 4 classes. It shows that the classes are meaningful, grouping together stalagmites based on their growth duration, hydroclimate, and geostatistical properties.

One class (represented in blue, Figure 12) comprises stalagmites with short growth duration or relatively low range, clustering all Ethiopian stalagmites with those from Molinos Cave and Akçakale Cave. Correlation of annual growth rate with instrumental temperature or precipitation records was weak or absent at Akçakale Cave (Jex, 2008) and Rukiesa Cave, Ethiopia (Baker et al., 2007). At Molinos Cave, thicker laminations grew during intervals characterized by more negative $\delta^{13}C$ values, and were darker in reflected light, interpreted as longer or more intense rainy winter-spring (Muñoz et al., 2015). Ethiopian stalagmites deposited during the Holocene and last Interglacial widely exhibit decadal-scale variability in growth rate, the cause of which is uncertain but considered to be hydroclimatically determined (Asrat et al., 2018; Baker et al., 2010).

The second MDS class (in magenta) groups long duration growth phases from water-limited environments: stalagmite samples from Carlsbad Cavern, USA and Kahf Defore, Oman; Gejkar Cave, Iraq and Shihua Cave, China. In monsoon climate regions, the Shihua Cave stalagmite has a growth rate record calibrated against rainfall and temperature (Tan et al., 2003). In the water-limited Carlsbad Cavern and Gejkar Cave records, annual growth rates vary with oxygen isotope ratio, and they are interpreted as records of moisture

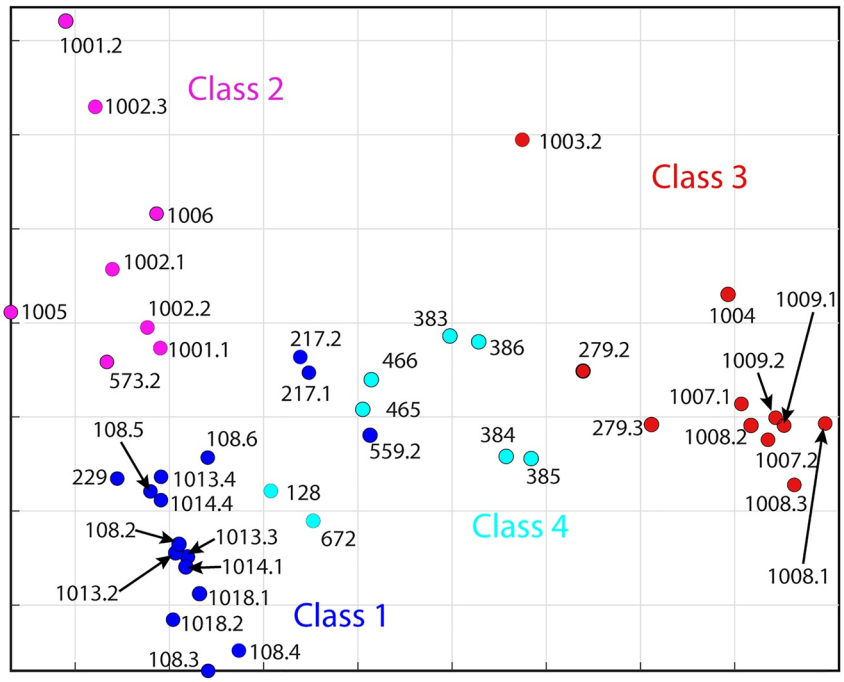

Figure 12. Multidimensional scaling with four clusters. Data included: growth rate; variogram properties range, sill, nugget, and information content (IC); flickering; mean annual temperature; total annual precipitation; potential evapotranspiration; Aridity Index, Precipitation Seasonality Index; modeled recharge, modeled soil and epikarst store percentage fullness, and the Recharge Seasonality Index. The distance chosen is the standardized Euclidean distance. The four clusters are coded by color and samples labeled by entity ID and growth phase (where relevant).

amount (Asmerom et al., 2013) or effective moisture and drip rates within the cave (Flohr et al., 2017), with thinner annual layers signifying reduced effective moisture.

The third class identified by the MDS (in red) groups growth phases with relatively high Information Content, from regions of water excess, predominantly alpine settings and peat-covered sites from Europe, such as Grotta di Ernesto, Uamh an Tartair, and Larsullet. Although not included in the MDS, this cluster is predominantly comprised of stalagmites with hydrological FOM and/or particulate organic matter laminae and high autocorrelation parameter τ. The Uamh an Tartair and Grotta di Ernesto stalagmite growth rate records from this group have growth rates which are sensitive to a NAO climate forcing (Baker et al., 2015; Frisia et al., 2003; Scholz et al., 2012). Both sites have low modern day drip water calcium concentrations that indicate that they are close to the edge of that possible for speleothem formation.

A fourth MDS class (in light blue) groups all the remaining stalagmites from China and SE Asia—six stalagmites from Qingtian Cave and Nuanhe Cave, China; the Tham Douan Mai Laotian stalagmite, and also the Brazilian Pau d'Alho Cave stalagmite. All are characterized by relatively long duration laminae sequences (shortest: 593 years) in regions with a highly seasonal, monsoonal climate with P/PET >0.8. At both Qingtian Cave and Nuanhe Cave, the authors report no correlation between annual growth rate and stalagmite $\delta^{18}O$ (Liu et al., 2015; Wu et al., 2012). This contrasts with MDS class 2, where stalagmites from water limited environments showed a correlation between growth rate and $\delta^{18}O$ (Asmerom et al., 2013; Flohr et al., 2017), likely due to the dominant control on growth rate of yearly seepage water amount. Wu et al. (2012) postulate that at Nuanhe Cave, that both drip water supersaturation and yearly seepage-water amount may determine annual growth rate, whereas stalagmite $\delta^{18}O$ in Chinese monsoon climate regions is more likely to relate to changes in moisture source of air masses interacting with the monsoon circulation (Hu et al., 2019).

4.2. Comparing Properties of Laminae Types: Fabric, POM, FOM, Sr

Our geostatistical analysis allows the comparison of the properties of different laminae types. We observed no difference in the flickering property, *f*, between laminae types. This inertia on growth rate changes is due to the properties of the water store feeding the stalagmite, and the similarity between lamina types suggests that although calcite fabric laminae might be determined by seasonal changes in cave climate and represent the cave climate year, the amount of annual vertical extension in that time period is predominantly controlled by hydroclimatic and karst hydrological processes.

We observe more variogram noise (or uncorrelated signal) where laminae are formed from changes in calcite fabric, and a greater information content (greater correlated signal to noise) in the variogram where the laminae formed from fluorescent organic matter. Stalagmites with laminae preserved through changes in calcite fabric occur at warmer and more water limited sites, where karst model output confirms that soil and epikarst stores are less full, allowing greater non-linear hydrological behavior over time and a greater probability of uncorrelated signal. Additionally, we propose that this greater noise found in the growth rate variogram for many sites with calcite fabric laminae is due to the cave climate year being asynchronous with the cave hydrological year. The modeled recharge for each of the sites is shown in Figure S1. Assuming the cave climate year commences around the spring or autumn equinox, then sites where increased recharge occurs at the same time could result in additional stalagmite growth in one of two laminae years, depending on the precise timing of recharge relative to change in ventilation. Sites particularly sensitive to this phenomenon include Carlsbad Cavern, USA, Actun Tunichil Muknal, Belize, Akçakale Cave, Turkey, Gejkar Cave, Iraq, and Pau d'Alho Cave, Brazil, where recharge maxima and minima occur at the equinoxes, and the Ethiopian caves, where there are two rainy seasons, one around the spring equinox. In contrast, where recharge has a large difference between summer versus winter seasons, recharge should consistently occur within one cave climate year and one laminae. Examples here include the Mediterranean climates types with dominant winter recharge (e.g., SW Australia), sites with summer monsoon rainfall dominating recharge (e.g., Qingtian Cave, China), and cool climate sites with relatively warm summer-limiting recharge (e.g., European sites Uamh an Tartair, Grotta di Ernesto, and Larshullet).

4.3. Paleoclimatically Sensitive Laminated Stalagmites

Stalagmites with demonstrated climate signal tend to fall into two groups (1) in water-limited environments, annual vertical extension or growth rate is limited by water availability, and growth rate records are interpreted as records of effective moisture and drip rates within the cave. Examples include records from Carlsbad Cavern, USA; Molinos Cave, Spain; and Gejkar Cave, Iraq. Where faster annual growth rates correlate with more negative $\delta^{18}O$ or $\delta^{13}C$ carbonate isotope composition, this helps confirm the likely hydrological control on the growth rate. (2) Stalagmites with a suitable hydrological connectivity (a high information content) from cooler or wetter climate regions, enabling a water excess and a seasonal soil hydrological connectivity indicated through fluorescent or colloidal-particulate rich laminae. They also appear to be located in caves where the climate is close to the limit of speleothem formation, which helps improve sensitivity to surface changes in climate and environment. Examples include records from the relatively winter-cold and summer-warm Uamh an Tartair, Scotland, and Grotta di Ernesto, Italy, sites.

Our geostatistical analysis suggests that there is a dominant hydrological buffering of the karst water store that limits growth rate variability over time, and that in many cases, this means that variations in stalagmite growth rate are complacent to climate variability (but still have value in geochronology, see Section 4.4). Over periods of significant global change, such as deglaciation, we hypothesize that the growth rate record could preserve evidence of climate change, where it changes the amount of water recharged to the karst stores feeding a hydrologically sensitive stalagmite, or significantly changes the chemistry of the buffering, stored water. With respect to climate phenomena that occur over multiyear or multidecadal timescales, stalagmites with the clearest evidence of climate forcing of growth rate have predominantly derived from regions with an ENSO or NAO control of temperature or rainfall, including monsoon strength. These include the instrumental calibration of growth rate to warm season temperature in Shihua Cave, Beijing (Tan et al., 2003) and instrumental calibration of a composite record from Uamh an Tartair, UK, against Jan-Mar precipitation, sea level pressure and the Jan–March NAO; Baker et al., 2015). This agrees with our observa-

tion that spectral power in the growth rate time series greater than a red noise signal mostly occur at periods <6 years. These observations suggest that possible regions for future research into stalagmite rate records that are sensitive to multiyear climate variations would include those with significant seasonal or annual temperature and precipitation variability influenced by phenomena such as the IOD, NAO, and ENSO. Another multiyear signal that may be preserved in the speleothem growth rate record is that of past fires. In forested regions, wildfire that destroys trees and shrubs can lead to a multiyear decrease in soil and vadose zone carbon dioxide production from root respiration (Coleborn et al., 2016), and a consequent decrease in drip water calcite supersaturation (Bian et al., 2019). Future research might investigate the extent to which stalagmites in fire-prone regions experience a decrease in growth rates over a multiyear time period.

4.4. Geochronological Characteristics of Laminated Stalagmites

For the majority of growth phases, and irrespective of depositional environment, we show that the age-depth relationship is linear ($R^2 > 0.967$) over the timescale of tens to thousands of years, which we interpret as due to the buffering effect of a well-mixed karst water store that is necessary to ensure continuous stalagmite deposition. This approximation to linearity can be used for geochronological applications.

Geochemical laminae can sometimes be hard to identify, obscured due to changes in elemental incorporation to different calcite fabric types (Borsato et al., 2019), the presence of fluid inclusions, porosity or crystal defects. This is especially problematic for line-scan techniques (e.g., by laser ablation mass spectrometry) which do not provide a 2-D spatial elemental map. It is reasonable to assume that linearity in vertical extension rate can help in the automation of peak detection as it can provide a range within which to identify peaks.

Linearity of laminated stalagmite vertical extension has utility when comparing laminae chronology to radiometric dating techniques, especially where laminated sequences have been rigorously checked for the absence of missing laminae and hiatuses. For example, ^{14}C analyses on speleothem presume a constant "dead" carbon proportion, and an assumption of a linear age-depth relationship can help constrain changes in dead carbon percentage and help quantify the use of ^{14}C when determining changes in past atmospheric ^{14}C. For U-Th dated laminated stalagmites, a linear age-depth relationship can be used to better constrain variations in $^{230}Th/^{232}Th$ detrital composition (Hellstrom, 2006; Linge et al., 2009). We do not observe the presence of growth rate changepoints close to growth terminations and hiatuses, and we can count laminae from the nearest U-Th dating location to obtain the start and end represented by a hiatus.

5. Conclusions

Globally, we observe that in relatively shallow caves (<100 m cover thickness) mean growth rate of stalagmite annual laminae changes with MAT and, therefore, with latitude and altitude. The median duration of laminated sequences is several hundred years, less in Ethiopia, where stalagmite deposition is constrained by regular tectonic activity on the East African Rift. Long-term growth rate is approximately linear, reflecting the buffering of the stored water required to maintain calcium carbonate deposition. At the year-to-year scale, growth rate deceleration back toward a mean state is ubiquitous as indicated by flickering, reflecting the inertia of the chemistry and volume of stored karst water. This phenomenon is observed irrespective of laminae type (fabric, particulate, fluorescent, or trace element). Spectral analysis of growth rate time series is largely identical to AR1 red noise. Spectral power greater than this red noise signal mostly occur at periods <6 years, reflecting a typical timescale where climate and/or environmental control on growth could be large enough to overcome the mixing of waters in the overlying karst stores. The geostatistical properties of laminated stalagmites represent the role karst hydrology and geochemistry and water stored in karstic voids or fractures, partially draining and refilling every year, providing a buffering and inertia to any changes in stalagmite growth rate. Again, spectral properties are similar for all laminae types, consistent with an overarching hydrological control on stalagmite annual growth rate, irrespective of whether laminae are physically or chemically preserved. Outliers in stalagmite flickering show some samples can have unique growth mechanisms, due to piston flow and seasonal dissolution. Geostatistical properties vary significantly between growth phases of individual stalagmite and between stalagmites at an individual site, indicating a

dominant drip-specific control due to drip specific hydrology. This points toward the value of replication of stalagmite growth rate records, within the practical limits imposed by conservation requirements.

At a global scale, MDS on all laminated stalagmite growth sequences does reveal clusters of stalagmites with similar properties (range, information content) and duration of laminated sequences, despite the drip-specific hydrological controls. These MDS clusters largely align with the extent of seasonal water limitation and with regions with tectonic controls on growth duration. In particular, samples with FOM or particulate organic matter laminae cluster with stalagmites with higher variogram information content, found in high latitude sites, alpine sites and monsoon sites with high recharge. Stalagmites with lower IC and greater variogram noise have fabric laminae and are largely found in water limited environments. Where the cave climate year as recorded by fabric laminae is asynchronous with the hydrological year, increased variogram noise can be introduced when small changes in recharge timing means that additional deposition occurs in different laminae years.

Despite the multiple processes that control stalagmite growth rate, their smoothing by the mixing of water in karst stores and fractures limits the temporal variability in growth rate, and changepoints between growth phases with significantly different mean growth rates are rare. This mixing and desire for the system to return to the dynamic equilibrium state of the stored water properties in general limits the climate information in the growth rate of annually laminated stalagmite time series, and explains why correlations between climate parameters and growth rate have proved to be the exception over multi-decadal time-scales. In contrast, laminated stalagmite growth rate time series would be expected to be sensitive to multiyear climate phenomena such as the IOD, ENSO, and NAO, especially in seasonally or annually water limited environments where moisture supply is the dominant control. Based on these findings, our recommendations for studies that utilize annual laminations for paleoclimatic purposes would be to target these regions. The broader application of laminated stalagmites is in their ability to provide an annually resolved chronology. The age-depth relationship of laminated stalagmites is close to linear over hundreds to thousands of years due to the smoothing/mixing effect of stored water on long-term growth rates. The long-term constant growth rate of laminated stalagmites advances their role in precise chronology building.

Glossary

Aeolianites: Rocks formed by the lithification of wind-transported sediments. Thus, if the cement is mostly calcium carbonate, even if the sediments consist of hardly soluble quartz, the rock may act as a karst rock.

Autocorrelation: Applied here to individual time series, the autocorrelation measures the linear relationship between different lagged values of the time series. Here, we consider the time series of annual vertical accumulation, or growth rate, of stalagmites. See also: variogram, red noise.

Changepoint: A statistical metric which identify times when the probability distribution of a stochastic process or time series changes. Here, it is applied to time series of stalagmite annual vertical accumulation, detecting whether or not a change has occurred in either mean or variance, and identifying the times of any such changes.

Diagenesis: Includes all those processes that occur soon after deposition and before metamorphism. In speleothems, diagenesis implies the transformation of aragonite into calcite or of vaterite into calcite and/or the dissolution of small calcite crystals and re-precipitation of larger calcite crystals. Diagenesis is not common in most speleothems, which is one of the greatest advantages of using stalagmites to investigate past climates.

El Niño-Southern Oscillation (ENSO): A climate phenomenon that changes the global circulation pattern over the Pacific Ocean and adjacent regions. During the El Niño, the Pacific Ocean surface warms over the central and eastern Pacific Ocean, resulting in drier conditions over Indonesia and Australia and wetter conditions over the tropical Pacific Ocean. In the La Niña, the cooling of the ocean surface in central and eastern tropical Pacific Ocean leads to drier conditions over the central tropic Pacific Ocean and wetter conditions in Indonesia and Australia. This cooling occurs typically every 3–7 years.

Epikarst: The epikarst is the near-surface few meters, or tens of meters, of a karstified rock such as limestone. At this shallow depth below surface, physical, and chemical weathering leads to enlargement of fractures and joints, which then promotes further dissolution of the karst rock by soil-derived carbonic acid. The epikarst therefore has numerous solution-widened fractures, which can temporarily store infiltrating rainwater thus retarding the time of transmission of the rainwater signal between the surface and the cave.

Fabric (stalagmite): Stalagmite fabric refers to the spatial orientation of the smallest crystal units that forms a stalagmite. Commonly, stalagmites are built by calcite crystals, which may be perfectly stacked one on top of the other if nothing disturbs the growth. But in caves there are many disturbances. Inflow of particulate from the soil disturbs the stacking, and may create pores between growing crystals. The addition of certain trace elements also disturbs the growth, because some elements influence the morphology of the growing crystals. Thus, the changes over time of stalagmite fabrics, provide insights into changes in the physical and chemical properties of the water from which the crystals form at seasonal to millennial timescales.

Flickering: **A** statistical metric describing the observed lag-one negative autocorrelation of growth increment, which is the change in growth rate from one year to the next. When the growth rate acceleration is strongly negative, high growth rate years tend to be followed by low growth years. This is termed as flickering and has been shown to be related to karst storage in Mariethoz et al. (2012). The occurrence of flickering is illustrated in Figure 13, where a portion of a stalagmite presenting a strong flickering pattern is zoomed in to show the oscillation between high and log growth in successive years.

Fluorescent organic matter (FOM): Aromatic carbon structures within natural organic matter can have the optical property of fluorescence, emitting light when excited by ultra-violet wavelength energy. Where natural organic matter is preserved within speleothem calcite, fluorescence microscopy allows the identification of the FOM.

Information content (IC): See variogram.

Indian Ocean Dipole (IOD): IOD is the difference between sea surface temperatures in the tropical western and eastern Indian Ocean. A positive IOD has warmer surface water adjacent to Africa, resulting in wetter conditions in NE Africa and drier conditions in the Australian region between May and December. The opposite occurs when there is a negative IOD. Since 1960, there have been 11 negative IOD and 10 positive IOD events.

Karst: It is the landforms associated with the dissolution of sparingly soluble rocks, most commonly carbonates (limestones and dolomites). Karstified carbonate rocks are characterized by focused recharge through closed depressions or sinkholes, the development of underground drainage systems, and lack of surface rivers and lakes. Caves containing stalagmites are typically part of this underground drainage system. When the system no longer floods, due to lower groundwater levels (or uplifted bedrock), passages are mostly filled by air and stalagmites form from percolating water.

LOWESS: A local regression technique, or moving regression, where a local weighting is applied. Here, it is used to detrend stalagmite annual vertical accumulation rate time series prior to analysis of changes in variance over time using changepoint analysis.

Multidimensional scaling (MDS): A visualization method to display the amount of similarity between samples of a data set. Here, the samples are the laminated stalagmite sequences, which form a global data set for which we have a large amount of different geostatistical and geospatial information. MDS is used to show this similarity between laminated stalagmite sequences mapped as a scatter plot in abstract two-dimensional space.

North Atlantic Oscillation (NAO): The NAO index is based on the surface sea-level pressure difference in the North Atlantic sector between the Subtropical High and the Subpolar Low. A positive NAO is associated with warmer temperatures in NE North America and North Europe, wetter conditions in northwest Europe and drier conditions in southern and central Europe. The opposite climate is experienced with a negative NAO. The NAO has high interannual variability, with prolonged periods of both positive and negative phases common.

Nugget: See variogram.

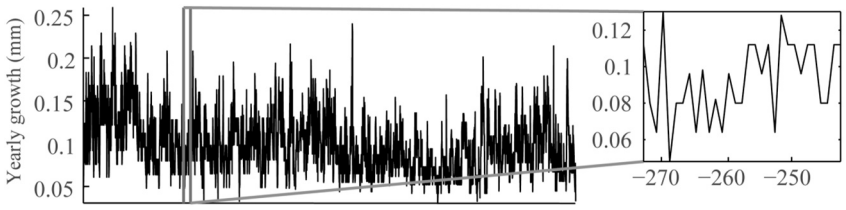

Figure 13. Example of flickering.

Pruned exact linear time (PELT): An algorithm to detect multiple changepoints in a time series. Changepoint detection methods comprise binary segmentation and segment neighborhood analyses. Binary segmentation uses a single changepoint test and a time series split into two segments. Each segment is then analyzed again, and this continues until no changepoints are detected. The algorithm is fast but only an approximation to the total number of changepoints. PELT is similar to the segment neighborhood algorithms, where dynamic programming is used to the optimal segmentation to detect all possible changepoints. These algorithms are exact but more computationally complex.

Prior calcite precipitation (PCP): A term used in speleothem science to describe the precipitation of calcite that has occurred along the water flow path prior to reaching the tip of a particular speleothem. Extensive PCP can result in a cave percolation water having a decreasing supersaturation with respect to calcite along a flowpath, and in the context of stalagmite growth properties, could be a factor determining annual vertical accumulation rate.

Range: See variogram.

Recharge: The movement of water to the groundwater. In the context of stalagmite percolation waters, the water is likely to have from rainfall, and it has yet to reach the groundwater, and it would be best defined as potential rainfall recharge. Recharge is modeled here using the Var-Karst model, which quantifies the monthly volume of water leaving the unsaturated zone.

Red noise: In time series analysis, this refers to the spectral analysis property where power density decreases with increasing frequency. In many paleoclimate proxies, including stalagmites, time series properties are autocorrelated, leading to a red noise spectrum. Here, we use the REDFIT software to specifically test whether time series of stalagmite annual vertical accumulation are different from an autoregression (1) or AR(1) function. That is, where the vertical accumulation at time t is related to the accumulation at time t minus 1, plus some noise.

Seasonality Index: Walsh and Lawler (1981) define a Seasonality Index as the sum of the absolute deviations of mean monthly rainfalls from the overall monthly mean, divided by the mean annual rainfall. If all months have equal rainfall, the index equals zero, and if all rainfall falls in 1 month, the index is 1.83: seasonality classes are defined by 0.2 index units. Here, we apply it to monthly precipitation to obtain a Precipitation Seasonality Index and to monthly modeled recharge to obtain a Recharge Seasonality Index.

Sill: See variogram.

Spectral analysis: In time series analysis, this is an algorithm that estimates the strength of different frequency components (the power spectrum). Specifically applied to stalagmites and other potential paleoclimate proxies, spectral analysis is used to elucidate frequencies (or periodicies) in a time series. Here, we investigate the time series of stalagmite annual vertical accumulation, to determine if there are frequencies that are statistically different from those that could be obtained from randomly generated AR(1) or red noise time series (see red noise).

Speleothem: A cave deposit (speleo—from ancient Greek spēlaion means cave; them—from the ancient Greek theme, which means the topic of/topic of). The use of them within the word speleothem has been transformed in the English language literature as signifying deposit.

Stalagmite: A chemical precipitate found in caves that forms from drip waters. It is a type of speleothem that accumulates from the cave floor in a vertical direction. It will typically have an associated stalactite, which forms on the cave ceiling and grows downward.

Synchrotron XRF: Synchrotron light is characterized by focused and high brilliance. X-rays (which we do not see) are emitted as part of the light spectrum and captured by a beamline in the desired range of wavelength and energy. These X-rays are so powerful that they can penetrate through thick stalagmite samples and reveal their chemical composition with an unparalleled accuracy.

Variogram: A geostatistical tool that describes the behavior of data, either spatially (2-D) or temporally correlated time series. Its principle is to compute the variance of pairs of data points that are separated by a certain lag (either a distance or a time-lag). The experimental variogram is the function that describes the observed variance for a series of increasing lags. This function typically increases with larger lags, as data become more decorrelated when their separation increases. A variogram model is a mathematical expression adjusted on the experimental variogram. The parameters values resulting from this adjustment provide information on the behavior of the observed variable, such as Range (r), Sill (c), and Nugget (n). The Range is related to the correlation length and can be seen as the persistence of episodes of thicker or thinner laminae; the Sill is the overall variance of the time series; the Nugget is the part of the signal that is unaccounted for by the range, and can be seen as uncorrelated signal; the Information Content which is the percentage of variance attributed to the correlated signal.

Vertical extension rate: Speleothem lamina thickness is measured as a distance from bottom to top of a growth lamina perpendicular to the lamina surface. It is a linear dimension and, as such, it is here referred to as vertical extension rate. This terminology prevents confusion with growth rate, which refers to the linear advancement of different calcite crystal faces. Different calcite crystal faces have different growth rate, and the result of growth rate differences is a three-dimensional calcite crystal. The growth rate of a calcite crystal is measured in the laboratory and is calculated in terms of mass deposited per unit area per unit time at a specified supersaturation. The area dimension is two dimensional, and time is the third dimension. When we measure the distance between top and bottom of a growth lamina in a stalagmite we are, practically, equating the vertical extension of the lamina with how fast the stalagmite grew per year. The extension rate accounts for the velocity at which a stalagmite layer grows in the vertical dimension (from floor to ceiling) and reflects not just calcite crystal growth, but also porosity and presence of impurities

White noise: In time series analysis, this refers to the spectral analysis property where power density does not vary with frequency. In other words, the time series has an autoregression 0 or AR(0) function. In terms of stalagmite deposition, it would mean that the vertical accumulation at time t is unrelated to the accumulation at any previous timesteps and comprises just noise. Here, we compare stalagmite flickering properties to white noise.

Conflict of Interest

The authors declare no conflicts of interest relevant to this study.

Data Availability Statement

Data sets for this research were extracted from the SISALv2 database (Comas-Bru, Atsawawaranunt, et al., 2020) and World Data Service for Paleoclimatology, part of the NOAA National Centers for Environmental Information (NCEI) repository (https://www.ncdc.noaa.gov/data-access/paleoclimatology-data/datasets/speleothem). The compiled data set, including four previously unpublished data, and electronic copies of tables, have been placed on Figshare (https://figshare.com/articles/dataset/Laminated_stalagmite_Dataset_csv/13166639).

Acknowledgments
This study includes data compiled by SISAL, a working group of the Past Global Changes (PAGES) project, which in turn received support from the Swiss Academy of Sciences and the Chinese Academy of Sciences.

References

Asmerom, Y., Polyak, V. J., Rasmussen, J. B. T., Burns, S. J., & Lachinet, M. (2013). Multidecadal to multicentury scale collapses of Northern Hemisphere monsoons over the past millennium. *Proceedings of the National Academy of Sciences of the United States of America*, *110*, 9651–9656.

Asrat, A. (2012). Speleoseismicity in the Mechara karst, Southeastern Ethiopia. In I. J. Fairchild & A. Baker (Eds.), (Eds). *Speleothem Science: From process to past environments*. Wiley-Blackwell.

Asrat, A., Baker, A., Leng, M. J., Hellstrom, J., Mariethoz, G., Boomer, I., et al. (2018). Paleoclimate change in Ethiopia around the last interglacial derived from annually-resolved stalagmite evidence. *Quaternary Science Reviews*, *202*, 197–210.

Badertscher, S., Borsato, A., Frisia, S., Cheng, H., Edwards, R. L., Tüysüz, O., & Fleitmann, D. (2014). Speleothems as sensitive recorders of volcanic eruptions – The Bronze Age Minoan eruption recorded in a stalagmite from Turkey. *Earth and Planetary Science Letters*, *392*, 58–66.

Bajo, S., Hellstrom, S., Frisia, S., Drysdale, S., Black, S., Woodhead, S., et al. (2016). "Cryptic" diagenesis and its implications for speleothem geochronologies. *Quaternary Science Reviews*, *148*, 17–28.

Baker, A., Asrat, A., Fairchild, I. J., Leng, M. J., Wynn, P. M., Bryant, C., et al. (2007). Analysis of the climate signal contained within $\delta^{18}O$ and growth rate parameters in two Ethiopian stalagmites. *Geochimica et Cosmochimica Acta*, *71*, 2975–2988.

Baker, A., Asrat, A., Leng, M., Thomas, L., Fairchild, I. J., Widmann, M., et al. (2010). Decadal-scale holocene climate variability recorded in an Ethiopian stalagmite. *The Holocene*, *20*, 827–836.

Baker, A., Flemons, I., Andersen, M. S., Coleborn, K., & Treble, P. C. (2016). What determines the calcium concentration of speleothem-forming drip waters? *Global and Planetary Change*, *143*, 152–161.

Baker, A., Genty, D., Dreybrodt, W., Barnes, W. L., Mockler, N. J., & Grapes, J. (1998). Testing theoretically predicted stalagmite growth rate with recent annually laminated samples: Implications for past stalagmite deposition. *Geochimica et Cosmochimica Acta*, *62*, 393–404.

Baker, A., Hellstrom, J. C., Kelly, B. F. J., Mariethoz, G., & Trouet, V. (2015). A composite annual-resolution stalagmite record of North Atlantic climate over the last three millennia. *Scientific Reports*, *5*, 10307.

Baker, A., Smart, P. L., Edwards, R. L., & Richards, D. A. (1993). Annual banding in a cave stalagmite. *Nature*, *364*, 518–520.

Bard, E., Hamelin, B. & Fairbanks, R. G. (1990). U-Th ages obtained by mass spectrometry in corals from Barbados: Sea level during the past 130,000 years. *Nature*, *346*, 456–458.

Barker, S., Knorr, G., Edwards, R. L., Parrenin, F., Putnam, A. E., Skinner, L. C., et al. (2011). 800,000 years of abrupt climate variability. *Science*, *334*, 347–351.

Belli, R., Frisia, S., Borsato, A., Drysdale, R., Hellstrom, J., Zhao, J. X., & Spötl, C. (2013). Regional climate variability and ecosystem responses to the last deglaciation in the northern hemisphere from stable isotope data and calcite fabrics in two northern Adriatic stalagmites. *Quaternary Science Reviews*, *72*, 146–158.

Berthelin, R., & Hartmann, A. (2020). The shallow subsurface of Karst systems: Review and directions. In C. Bertrand, S. Denimal, M. Steinmann, & P. Renard (Eds.), *Advances in Karst science* (pp. 61–68). Cham, Switzerland: Springer International Publishing.

Bian, F., Coleborn, K., Flemons, I., Baker, A., Treble, P. C., Hughes, C. E., et al. (2019). Hydrological and geochemical responses of fire in a shallow cave system. *Science of the Total Environment*, *662*, 180–191.

Black, D. E., Abahazi, M. A., Thunell, R. C., Kaplan, A., Tappa, E. J. & Peterson, L. C. (2007). An 8-century tropical Atlantic SST record from the Cariaco Basin: Baseline variability, twentieth-century warming, and Atlantic hurricane frequency. *Paleoceanography and Paleoclimatology*, *22*, PA4204. https://doi.org/10.1029/2007PA001427

Borsato, A., Frisia, S., Fairchild, I. J., Somogyi, A., & Susini, J. (2007). Trace element distribution in annual stalagmite laminae mapped by micrometer-resolution X-ray fluorescence: Implications for incorporation of environmentally significant species. *Geochimica et Cosmochimica Acta*, *71*, 1494–1512.

Borsato, A., Frisia, S., Hellstrom, J., Treble, P., Johnson, K., Howard, D., & Greig, A. (2019). *Fast high-resolution synchrotron micro-XRF mapping of annually laminated stalagmites*. EGU General Assembly Geophysical Research Abstracts, EGU2019, 21.

Borsato, A., Frisia, S., & Miorandi, R. (2015). Carbon dioxide concentration in temperate climate caves and parent soils over an altitudinal gradient and its influence on speleothem growth and fabrics. *Earth Surface Processes and Landforms*, *40*, 1158–1170.

Borsato, A., Johnston, V. E., Frisia, S., Miorandi, R., & Corradini, F. (2016). Temperature and altitudinal influence on karst dripwater chemistry: Implications for regional-scale palaeoclimate reconstructions from speleothems. *Geochimica et Cosmochimica Acta*, *177*, 275–297.

Brauer, A., Haug, G. H., Dulski, P., Sigman, D. M., & Negendank, J. F. (2008). An abrupt wind shift in western Europe at the onset of the Younger Dryas cold period. *Nature Geoscience*, *1*, 520–523.

Broecker, W. S., Olson, E. A., & Orr, P. C. (1960). Radiocarbon measurement and annual rings in cave formations. *Nature*, *185*, 93–94.

Brook, E. J., & Buizert, C. (2018). Antarctic and global climate history viewed from ice cores. *Nature*, *558*, 200–208.

Brook, G. A., Folkoff, M. E., & Box, E. O. (1983). A world model of soil carbon dioxide. *Earth Surface Processes and Landforms*, *8*, 79–88.

Brook, G. A., Rafter, M. A., Railsback, L. B., Sheen, S. -W. & Lundberg, J. (1999). A high-resolution proxy record of rainfall and ENSO since AD 1550 from layering in stalagmites from Anjohibe Cave, Madagascar. *The Holocene*, *9*, 695–705.

Buhmann, D., & Dreybrodt, W. (1985). The kinetics of calcite dissolution and precipitation in geologically relevant situations of karst areas: I Open System. *Chemical Geology*, *48*, 189–211.

Coleborn, K., Spate, A., Tozer, M., Treble, P. C., Andersen, M. S., Fairchild, I. J., et al. (2016). Effects of wildfire on long-term soil CO_2 concentration: Implications for karst processes. *Environmental Earth Sciences*, *75*, 330.

Comas-Bru, L., Atsawawaranunt, K., & Harrison, S., & SISAL working group members. (2020b). SISAL (Speleothem isotopes synthesis and AnaLysis working group) Database version 2.0. University of Reading. Dataset. Retrieved from http://dx.doi.org/10.17864/1947.256

Comas-Bru, L., Rehfeld, K., Roesch, C., Amirnezhad-Mozhdehi, S., Harrison, S. P., Atsawawaranunt, K., et al. (2020a). SISALv2: A comprehensive speleothem isotope database with multiple age-depth models. *Earth System Science Data*, *12*, 2579–2606.

Davis, K. J., Dove, P. M., & De Yoreo, J. J. (2000). The role of Mg^{2+} as an impurity in calcite growth. *Science*, *290*, 1134–1137.

Demény, A., Németh, A., Kern, Z., Czuppon, G., Molnár, M., Leél-Ossy, S., et al. (2017). Recently forming stalagmites from the Baradla Cave and their suitability assessment for climate-proxy relationships. *Central European Geology*, *60*, 1–34.

Dominguez-Villar, D., Baker, A., Fairchild, I. J. & Edwards, R. L. (2012). A method to anchor floating chronologies in annually laminated speleothems with U-Th dates. *Quaternary Geochronology*, *14*, 57–66.

Dreybrodt, W. (1999). Chemical kinetics, speleothem growth and climate. *Boreas*, *28*, 347–356.

Drysdale, R. N., Hellstrom, J. C., Zanchetta, G. I., Fallick, A. E., Goñi, M. S., Couchoud, I., et al. (2009). Evidence for obliquity forcing of glacial termination II. *Science*, *325*, 1527–1531.

Drysdale, R. N., Zanchetta, G., Hellstrom, J. C., Fallick, A. E., McDonald, J., & Cartwright, I. (2007). Stalagmite evidence for the precise timing of North Atlantic cold events during the early last glacial. *Geology*, *35*, 77–80.

Duan, W., Cai, B., Tan, M., Liu, H., & Zhang, Y. (2012). The growth mechanism of the aragonitic stalagmite laminae from Yunnan Xianren Cave, SW China revealed by cave monitoring. *Boreas*, *41*, 113–123.

Fairchild, I. J., & Baker, A. (2012). *Speleothem science: From process to past environments*. Wiley-Blackwell.

Fairchild, I. J., Baker, A., Borsato, A., Frisia, S., Hinton, R. W., McDermott, F., & Tooth, A. F. (2001). Annual to sub-annual resolution of multiple trace-element trends in speleothems. *Journal of the Geological Society, London*, *158*, 831–841.

Fleitmann, D., Burns, S. J., Neff, U., Mudelsee, M., Mangini, A., & Matter, A. (2004). Paleoclimate interpretation of high-resolution oxygen isotope profiles derived from annually laminated speleothems from Southern Oman. *Quaternary Science Reviews*, *23*, 935–945.

Flohr, P., Fleitmann, D., Zorita, E., Sadekov, A., Cheng, H., Bosomworth, M., et al. (2017). Late Holocene droughts in the Fertile Crescent recorded in a speleothem from northern Iraq. *Geophysical Research Letters*, *44*, 1528–1536. https://doi.org/10.1002/2016GL071786

Frappier, A., Sahagian, D., Carpenter, S. J., Gonzalex, L. A., & Frappier, B. R. (2007). Stalagmite stable isotope record of recent tropical cyclone events. *Geology*, *35*, 111–114.

Frisia, S., Borsato, A., Fairchild, I. J. & McDermott, F. (2000). Calcite fabrics, growth mechanisms and environments of formation in speleothems from the Italian Alps and southwest Ireland. *Journal of Sedimentary Research*, *70*, 1183–1196.

Frisia, S., Borsato, A., Preto, N., & McDermott, F. (2003). Late Holocene annual growth in three Alpine stalagmites records the influence of solar activity and the North Atlantic Oscillation on winter climate. *Earth and Planetary Science Letters*, *216*, 411–424.

Genty, D. (1993). Seasonal alternations in the internal structure of stalagmites: Importance for the reconstitution of continental palaeoenvironments. *Comptes Rendus de l'Académie des Sciences Série II*, *317*, 1229–1236.

Goldscheider, N., Chen, Z., Auler, A. S., Bakalowicz, M., Broda, S., Drew, D., et al. (2020). Global distribution of carbonate rocks and karst water resources. *Hydrogeology Journal*, *28*, 1661–1677. https://doi.org/10.1007/s10040-020-02139-5

Hargreaves, G. L., Hargreaves, G. H., & Riley, J. P. (1985). Irrigation water requirements for Senegal River Basin. *Journal of Irrigation and Drainage Engineering*, *111*, 265–275.

Harris, I., Osborn, T. J., Jones, P., & Lister, D. (2020). Version 4 of the CRU TS monthly high-resolution gridded multivariate climate dataset. *Scientific Data*, *7*, 109.

Hartmann, A., & Baker, A. (2017). Modeling karst vadose zone hydrology and its relevance for paleoclimate reconstruction. *Earth-Science Reviews*, *172*, 178–192.

Hartmann, A., Liu, Y., Olarinoye, T., Berthelin, R., & Marx, V. (2020). Integrating field work and large-scale modeling to improve assessment of karst water resources. *Hydrogeology Journal*, *29*, 315–329. https://doi.org/10.1007/s10040-020-02258-z

Hellstrom, J. (2006). U–Th dating of speleothems with high initial ^{230}Th using stratigraphical constraint. *Quaternary Geochronology*, *1*, 289–295.

Holmgren, K., Lauritzen, S. E., & Possnert, G. (1994). ^{230}Th-^{234}U and ^{14}C dating of a late Pleistocene stalagmite in Lobatse II Cave, Botswana. *Quaternary Science Reviews*, *13*, 111–119.

Hua, Q., McDonald, J., Redwood, D., Drysdale, R., Lee, S., Fallon, S., & Hellstrom, J. (2012). Robust chronological reconstruction for young speleothems using radiocarbon. *Quaternary Geochronology*, *14*, 67–80.

Hu, J., Emile-Geay, J., Tabor, C., Nusbaumer, J., & Partin, J. (2019). Deciphering oxygen isotope records from Chinese speleothems with an isotope-enabled climate model. *Paleoceanography and Paleoclimatology*, *34*, 2098–2112. https://doi.org/10.1029/2019PA003741

James, E. W., Banner, J. L., & Hardt, B. (2015). A global model for cave ventilation and seasonal bias in speleothem paleoclimate records. *Geochemistry, Geophysics, Geosystems*, *16*, 1044–1051. https://doi.org/10.1002/2014GC005658

Jean-Baptiste, P., Genty, D., Fourre, E., & Regnier, E. (2019). Tritium dating of dripwater from Villars Cave (SW-France). *Applied Geochemistry*, *107*, 152–158.

Jex, C. N. (2008). *Speleothem palaeoclimate reconstructions from Northeast Turkey* (Unpublished PhD thesis). University of Birmingham.

Jex, C. N., Baker, A., Eden, J. M., Eastwood, W. J., Fairchild, I. J., Leng, M. J., et al. (2011). A 500 yr speleothem-derived reconstruction of late autumn-winter precipitation, North East Turkey. *Quaternary Research*, *75*, 399–405.

Jex, C. N., Mariethoz, G., Baker, A., Graham, P., Andersen, M. S., Acworth, I., et al. (2012). Spatially dense drip hydrological monitoring and infiltration behaviour at the Wellington Caves, South East Australia. *International Journal of Speleology*, *41*, 285–298.

Kaufman, A., Bar-Matthews, M., Ayalon, A., & Carmi, I. (2003). The vadose flow above Soreq Cave, Israel: A tritium study of the cave waters. *Journal of Hydrology*, *273*, 155–163.

Killick, R., Fearnhead, P., & Eckley, I. A. (2012). Optimal detection of changepoints with a linear computational cost. *Journal of the American Statistical Association*, *107*, 1590–1598.

Kluge, T., Riechelmann, D. F. C., Wieser, M., Spotl, C., Sultenfuss, J., Schroder-Ritzrau, A., et al. (2010). Dating cave drip water by tritium. *Journal of Hydrology*, *394*, 396–406.

Lemieux-Dudon, B., Blayo, E., Petit, J. R., Waelbroeck, C., Svensson, A., Ritz, C., et al. (2010). Consistent dating for Antarctic and Greenland ice cores. *Quaternary Science Reviews*, *29*, 8–20.

Linge, H., Baker, A., Andersson, C., & Lauritzen, S. E. (2009). Variable luminescent lamination and initial ^{230}Th/^{232}Th activity ratios in a late Holocene stalagmite from northern Norway. *Quaternary Geochronology*, *4*, 181–192.

Liu, D., Wang, Y., Cheng, H., Edwards, R. L., & Kong, X. (2015). Cyclic changes of Asian monsoon intensity during the early mid-Holocene from annually-laminated stalagmites, central China. *Quaternary Science Reviews*, *121*, 1–10.

Mariethoz, G., Kelly, B., & Baker, A. (2012). Quantifying the value of laminated stalagmites for paleoclimate reconstructions. *Geophysical Research Letters*, *39*, L05407. https://doi.org/10.1029/2012GL050986

Martens, B., Miralles, D. G., Lievens, H., Van Der Schalie, R., De Jeu, R. A. M., Fernández-Prieto, D., et al. (2017). GLEAM v3: Satellite-based land evaporation and root-zone soil moisture. *Geoscientific Model Development*, *10*, 1903–1925.

Mattey, D., Lowry, D., Duffet, J., Fisher, R., Hodge, E., & Frisia, S. (2008). A 53 year seasonally resolved oxygen and carbon isotope record from a modern Gibraltar speleothem: Reconstructed drip water and relationship to local precipitation. *Earth and Planetary Science Letters*, *269*, 80–95.

Mattey, D. P., Fairchild, I. J., Atkinson, T. C., Latin, J. -P., Ainsworth, M. & Durell, R. (2010). Seasonal microclimate control of speleothem fabrics, stable isotopes and trace elements in modern speleothem from St Michaels Cave, Gibraltar. *Geological Society, London, Special Publications*, *336*, 323–344.

Miralles, D. G., Holmes, T. R. H., De Jeu, R. A. M., Gash, J. H., Meesters, A. G. C. A., & Dolman, A. J. (2011). Global land-surface evaporation estimated from satellite-based observations. *Hydrology and Earth System Sciences*, *15*, 453–469.

Muñoz, A., Bartolomé, M., Muñoz, A., Sancho, C., Moreni, A., Hellstrom, J. C., et al. (2015). Solar influence and hydrological variability during the Holocene from a speleothem annual record (Molinos Cave, NE Spain). *Terra Nova*, *27*, 300–311.

Muscheler, R., Kromer, B., Björck, S., Svensson, A., Friedrich, M., Kaiser, K. F., & Southon, J. (2008). Tree rings and ice cores reveal ^{14}C calibration uncertainties during the Younger Dryas. *Nature Geoscience*, *1*, 263–267.

Myers, C. G., Oster, J. L., Sharp, W. D., Bennartz, R., Kelley, N. P., Covey, A. K., & Breitenbach, S. F. M. (2015). Northeast Indian stalagmite records Pacific decadal climate change: Implications for moisture transport and drought in India. *Geophysical Research Letters*, *42*, 4124–4132. https://doi.org/10.1002/2015GL063826

Nagra, G., Treble, P. C., Andersen, M. S., Bajo, P., Hellstrom, J., & Baker, A. (2017). Dating stalagmites in mediterranean climates using annual trace element cycles. *Scientific Reports*, *7*(1), 1–12.

Novello, V. F., Vuille, M., Cruz, F. W., Stríkis, N. M., Saito de Paula, M., Edwards, R. L., et al. (2016). Centennial-scale solar forcing of the South American monsoon system recorded in stalagmites. *Scientific Reports*, *6*, 24762.

Orland, I. J., Burstyn, Y., Bar-Matthews, M., Kozdon, R., Ayalon, A., Matthews, A., & Valley, J. W. (2014). Seasonal climate signals (1990–2008) in a modern Soreq Cave stalagmite as revealed by high-resolution geochemical analysis. *Chemical Geology*, *363*, 322–333.
Parrenin, F., Barnola, J. M., Beer, J., Blunier, T., Castellano, E., Chappellaz, J., et al. (2007). The EDC3 chronology for the EPICA Dome C ice core. *Climate of the Past*, *3*, 485–497.
Peterson, L. C., & Haug, G. H. (2006). Variability in the mean latitude of the Atlantic Intertropical Convergence Zone as recorded by riverine inputs of sediments to the Cariaco Basin (Venezuela). *Paleogeography, Paleoclimatology, Paleoecology*, *234*, 97–113. https://doi.org/10.1016/j.palaeo.2005.10.021
Peterson, L. C., Haug, G. H., Hughen, K. A., & Röhl, U. (2000). Rapid changes in the hydrologic cycle of the tropical Atlantic during the last glacial. *Science*, *390*, 1947–1951.
Proctor, C. J., Baker, A., & Barnes, W. L. (2002). A three thousand year record of North Atlantic climate. *Climate Dynamics*, *19*, 449–454.
Rasbury, M., & Aharon, P. A. (2006). ENSO-controlled rainfall variability records archived in tropical stalagmites from the mid-ocean island of Niue, South Pacific. *Geochemistry, Geophysics, Geosystems*, *7*, Q07010. https://doi.org/10.1029/2005GC001232
Rasmussen, J. B. T., Polyak, V. J., & Asmerom, Y. (2006). Evidence for Pacific-modulated precipitation variability during the late Holocene from the southwestern USA. *Geophysical Research Letters*, *33*, L08701. https://doi.org/10.1029/2006GL025714
Ridley, H. E., Amserom, Y., Baldini, J. U. L., Breitenbach, S. F. M., Aquino, V. V., Prufer, K. M., et al. (2015). Aerosol forcing of the position of the intertropical convergence zone since AD 1550. *Nature Geoscience*, *8*, 195–200.
Roberts, M. S., Smart, P. L., & Baker, A. (1998). Annual trace element variations in a Holocene speleothem. *Earth and Planetary Science Letters*, *154*, 237–246.
Rodell, B. Y. M., Houser, P. R., Jambor, U., Gottschalck, J., Mitchell, K., Meng, C.-J., et al. (2004). The global land data assimilation system. *Bulletin of the American Meteorological Society*, *85*, 381–394.
Roig, F. A., Le-Quesne, C., Boninsegna, J. A., Briffa, K. R., Lara, A., Grudd, H., et al. (2001). Climate variability 50,000 years ago in mid-latitude Chile as reconstructed from tree rings. *Nature*, *410*, 567–570.
Scholz, D., Frisia, S., Borsato, A., Spotl, C., Fohlmeister, J., Mudelsee, M., et al. (2012). Holocene climate variability in north-eastern Italy: Potential influence of the NAO and solar activity recorded by speleothem data. *Climate of the Past*, *8*, 1367–1383.
Schulz, M., & Mudelsee, M. (2002). REDFIT: Estimating red-noise spectra directly from unevenly paced paleoclimatic time series. *Computers & Geosciences*, *28*, 421–426.
Shopov, Y. Y., Ford, D. C., & Schwarz, H. P. (1994). Luminescent microbanding in speleothems – High-resolution chronology and paleoclimate. *Geology*, *22*, 407–410.
Sirocko, F., Dietrich, S., Veres, D., Grootes, P. M., Schaber-Mohr, K., Seelos, K., et al. (2013). Multi-proxy dating of Holocene maar lakes and Pleistocene dry maar sediments in the Eifel, Germany. *Quaternary Science Reviews*, *62*, 56–76.
Smith, C. L., Fairchild, I. J., Spötl, C., Frisia, S., Borsato, A., Moreton, S. G., & Wynn, P. M. (2009). Chronology-building using objective identification of annual signals in trace element profiles of stalagmites. *Quaternary Geochronology*, *4*, 11–21.
Staubwasser, M., Sirocko, F., Grootes, P. M., & Segl, M. (2003). Climate change at the 4.2 ka BP termination of the Indus valley civilisation and Holocene South Asian monsoon variability. *Geophysical Research Letters*, *30*, 1425. https://doi.org/10.1029/2002GL016822
Tan, M., Liu, T., Hou, J., Qin, X., Zhang, H., & Li, T. (2003). Cyclic rapid warming on centennial scale revealed by a 2650-year stalagmite record of warm season temperature. *Geophysical Research Letters*, *30*, 1617. https://doi.org/10.1029/2003GL017352
Tierney, J. E., Abram, N. J., Anchukaitis, K. J., Evans, M. N., Giry, C., Halimeda Kilbourne, K., et al. (2015). Tropical sea surface temperatures for the past four centuries reconstructed from coral archives. *Paleoceanography and Paleoclimatology*, *30*, 226–252. https://doi.org/10.1002/2014PA002717
Treble, P. C., Chappell, J., Gagan, M. K., McKeegan, K. D., & Harrison, T. M. (2005). In situ measurement of seasonal delta O-18 variations and analysis of isotopic trends in a modem speleothem from southwest Australia. *Earth and Planetary Science Letters*, *233*, 17–32.
Trouet, V., Esper, J., Graham, N. E., Baker, A., Scourse, J. D., & Frank, D. C. (2009). Persistent positive North Atlantic Oscillation mode dominated the Medieval Climate Anomaly. *Science*, *324*, 78–80.
Vaks, A., Mason, A. J., Breitenbach, S. F. M., Kononov, A. M., Osinzev, A. V., Rosensaft, M., et al. (2020). Paleoclimate evidence of vulnerable permafrost during times of low sea ice. *Nature*, *577*, 221–225.
Walsh, R. P. D., & Lawler, D. M. (1981). Rainfall seasonality: Description, spatial patterns and change through time. *Weather*, *36*, 201–208.
Wang, J. K., Johnson, K. R., Borsato, A., Amaya, D. J., Griffiths, M. L., Henderson, G. M., et al. (2019). Hydroclimatic variability in southeast Asia over the past two millennia. *Earth and Planetary Science Letters*, *525*, 115737.
Williams, P. W. (1983). The role of the subcutaneous zone in karst hydrology. *Journal of Hydrology*, *61*, 45–67.
Wolff, C., Haug, G. H., Timmerman, A., Sinninghe Damsté, J. S., Brauer, A., Sigman, D. M., et al. (2011). Reduced interannual rainfall variability in East Africa during the last ice age. *Science*, *333*, 743–747.
Woodhead, J., Reisz, R., Fox, D., Drysdale, R., Hellstrom, J., Maas, R., et al. (2010). Speleothem climate records from deep time? Exploring the potential with an example from the Permian. *Geology*, *38*, 455–458.
Woodhead, J. D., Sniderman, J. M. K., Hellstrom, J., Drysdale, R. N., Maas, R., White, N., et al. (2019). The antiquity of Nullarbor speleothems and implications for karst palaeoclimate archives. *Scientific Reports*, *9*, 603.
Wu, J. Y., Wang, Y. J., Cheng, H., Kong, X. G., & Liu, D. B. (2012). Stable isotope and trace element investigation of two contemporaneous annually-laminated stalagmites from northeastern China surrounding the 8.2 ka event. *Climate of the Past*, *8*, 1497–1507.
Zolitschka, B., Francus, P., Ojala, A. E., & Schimmelmann, A. (2015). Varves in lake sediments – A review. *Quaternary Science Reviews*, *117*, 1–41.
Zomer, R. J., Bossio, D. A., Trabucci, A., Yuanjie, L., Gupta, D. C., & Singh, V. P. (2007). *Trees and water: Smallholder agroforestry on irrigated lands in Northern India*. Colombo, Sri Lanka: International Water Management Institute.
Zomer, R. J., Trabucco, A., Bossio, D. A., van Straaten, O., & Verchot, L. V. (2008). Climate change mitigation: A spatial analysis of global land suitability for clean development mechanism afforestation and reforestation. *Agriculture, Ecosystems & Environment*, *126*, 67–80.